

Modern Scattering-Type Scanning Near-Field Optical Microscopy for Advanced Material Research

Xinzhong Chen, Debo Hu, Ryan Mescall, Guanjun You, D. N. Basov,* Qing Dai,* and Mengkun Liu*

Infrared and optical spectroscopy represents one of the most informative methods in advanced materials research. As an important branch of modern optical techniques that has blossomed in the past decade, scattering-type scanning near-field optical microscopy (s-SNOM) promises deterministic characterization of optical properties over a broad spectral range at the nanoscale. It allows ultrabroadband optical (0.5–3000 μm) nanoimaging, and nanospectroscopy with fine spatial (<10 nm), spectral (<1 cm^{-1}), and temporal (<10 fs) resolution. The history of s-SNOM is briefly introduced and recent advances which broaden the horizons of this technique in novel material research are summarized. In particular, this includes the pioneering efforts to study the nanoscale electrodynamic properties of plasmonic metamaterials, strongly correlated quantum materials, and polaritonic systems at room or cryogenic temperatures. Technical details, theoretical modeling, and new experimental methods are also discussed extensively, aiming to identify clear technology trends and unsolved challenges in this exciting field of research.

(s-SNOM), have undergone tremendous development. This development has been partly driven by the ever-increasing demand for the exploration of the nano-world and partly attributed to the many technical advances in laser and scanning probe technology. The wavelength-independent spatial resolution of s-SNOM goes far beyond the Abbe diffraction limit,^[1,2] with numerous applications in material characterization throughout the fields of physics,^[3–7] chemistry,^[8–14] biology,^[10,15–25] engineering,^[26–32] and geo- and space-related sciences.^[33] The phase-sensitive detection methods provide new opportunities to study electromagnetic (EM) mode dispersion, light-matter interaction, and electron-lattice correlation at nanoscale resolutions, which conventional microscopy techniques, such as

1. Introduction

Over the past decade, optical near-field techniques, especially scattering-type scanning near-field optical microscopy

phase contrast microscopy,^[34,35] differential interference contrast microscopy,^[36] and laser scanning confocal microscopy,^[37] fail to easily achieve.

To conceptually interpret the fundamental difference between a conventional far-field optical measurement and a near-field measurement, one can imagine a simple scattering experiment with a macroscopic object, as illustrated in **Figure 1**. In general, the optical properties of this object can be characterized by the position (\mathbf{r})-, frequency (ω)-, and momentum (\mathbf{q})-dependent optical dielectric constant $\epsilon(\mathbf{r}, \omega, \mathbf{q})$. A light source far from the object generates propagating EM radiation (blue) that illuminates the object in free space. Upon illumination, the object induces a propagating field (blue) and a nonradiating field (yellow),^[38] and the latter decays exponentially normal to the sample surface. For infrared (IR) illumination, the nonradiating field dies off typically within tens to hundreds of nanometers^[39] in the so-called near-field zone. The propagating field, on the contrary, can radiate into free space and be collected by a detector far from the object. By analyzing the detected far-field signal, the material characteristics of the object, such as the complex dielectric permittivity (or equivalently, complex optical conductivity, or index of refraction), can be inferred based on classical EM theory.^[40] However, limited by diffraction, the focused spot size of illumination is fundamentally prohibited from being much smaller than the wavelength. Consequently, the detected signal is insensitive to local variations in the object at a subwavelength scale. More importantly, the information contained in the nonradiating near field, which might encode

X. Chen, R. Mescall, Prof. M. Liu
Department of Physics and Astronomy
Stony Brook University
Stony Brook, NY 11794, USA
E-mail: mengkun.liu@stonybrook.edu

Dr. D. Hu, Prof. Q. Dai
Division of Nanophotonics
CAS Center for Excellence in Nanoscience
National Center for Nanoscience and Technology
Beijing 100190, China
E-mail: daiq@nanoctr.cn

Prof. G. You
Shanghai Key Lab of Modern Optical Systems and Engineering Research
Center of Optical Instrument and System
Ministry of Education
University of Shanghai for Science and Technology
Shanghai 200093, China

Prof. D. N. Basov
Department of Physics
Columbia University
New York, NY 10027, USA
E-mail: db3056@columbia.edu

 The ORCID identification number(s) for the author(s) of this article can be found under <https://doi.org/10.1002/adma.201804774>.

DOI: 10.1002/adma.201804774

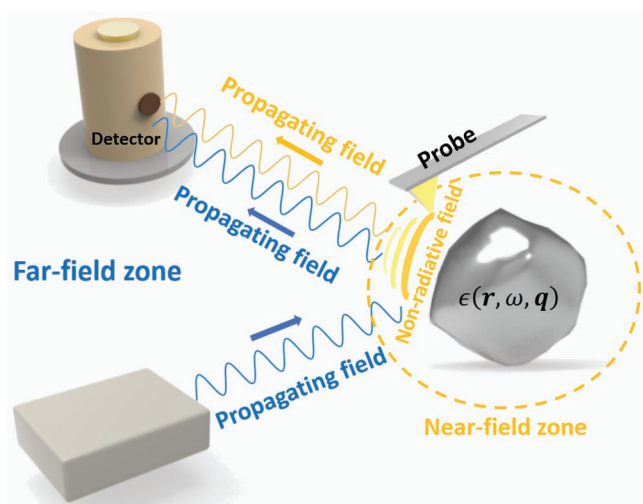
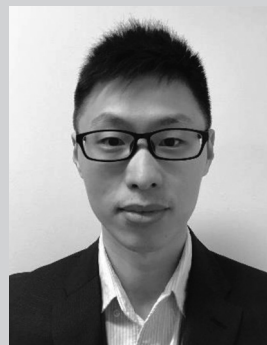


Figure 1. Far-field (blue) and near-field (yellow) measurements, accessing the propagating field and the evanescent field, respectively.

the important high spatial frequency (momentum) properties of the object, is completely lost. The objective of near-field measurements is to retrieve lost information with a spatial resolution not defined by free space optics. However, to achieve this goal, several tradeoffs must be made. Notably, a sharp probe must be placed near the sample surface, and a more complicated sample-probe ensemble is required instead using a simple isolated sample system. Additionally, fully understanding the optical properties of the probe can be challenging, as a probe can function as a light confiner (due to the extremely small radius of curvature of the apex) and a scatterer (partly due to its elongated shape, which is analogous to that of an antenna). Furthermore, the nonradiating field directly modifies the probe polarizability, which eventually manifests itself in the far-field-detectable wave (yellow) in a nontrivial way. With carefully executed experiments and theoretical treatments, object surface information at a small length scale can be accessed. For a more in-depth analysis and additional physical insight into the fundamental characteristics of near-field optics, readers are directed to references.^[41–43]

s-SNOM is a scanning technique that encompasses these concepts. In this technique, the sample is raster scanned under an oscillating probe (commonly referred to as “the tip”) of an atomic force microscope (AFM). The probe serves as a nanoscale light confiner, enhancer, and scatterer. Compared to other scanning techniques, such as scanning electron microscopy (SEM),^[44] scanning tunneling microscopy (STM),^[45] and scanning transmission electron microscopy (STEM),^[46] s-SNOM offers different dominant contrast. Specifically, this approach yields optical properties (e.g., dielectric constants) beyond the diffraction limit with compatible spectroscopic capability and temporal sensitivity. At the same time, the AFM tip serves as a light momentum matcher, which enables momentum (q)-resolved optical characterization, typically on the order of 10 to 100 nm⁻¹ based predominantly on the dimensions of the tip.^[47]

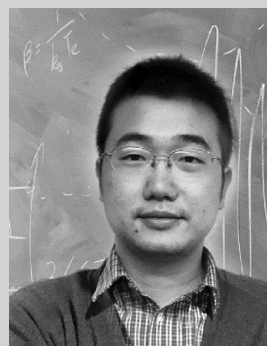
Like in any other tip-based scanning technique, the collected information is difficult to interpret due to nontrivial



Xinzhong Chen is a Ph.D. student working under Prof. Mengkun Liu’s supervision in the Department of Physics and Astronomy, Stony Brook University. His main research focuses include probing strongly correlated electron systems with near-field optics and developing next-generation near-field optical microscopy instruments.



Qing Dai is a professor of the National Center of Nanoscience and Technology, China. He received his B.Eng. and M.Eng. in electronic and electrical engineering from Imperial College, London in 2007 and Ph.D. in nanophotonics from the Department of Engineering, University of Cambridge in 2011. His main research interests are low-dimensional materials, optoelectronics, nanophotonics, and near-field optical characterization.



Mengkun Liu received a Ph.D. degree in physics from Boston University, MA, USA, in 2012. In 2015, he joined Stony Brook University, Stony Brook, NY, USA, as an Assistant Professor with the Department of Physics and Astronomy. His research interests cover nanoscale and ultrafast electromagnetic responses of strongly correlated electron materials, 2D materials, and metamaterials that span from the near-infrared to terahertz frequencies.

tip-sample interactions. In s-SNOM, these difficulties result from at least three factors. First, the well-known antenna effect^[48] causes light to be highly confined between the probe apex and the sample surface. The specific geometry of the tip shank plays a significant role in determining the intensity of the scattered signal.^[49] Second, in addition to the local optical information, a strong but undesired background signal can be detected. This background signal can be mainly attributed to the light scattering from the tip shank, cantilever, and sample surface. Third, due to the broad momentum distribution of the localized radiation, in some cases, nominally “far-field trivial”

phenomena such as the nonlocality of electrons and phonons must be carefully addressed.^[50,51] These complications can occur in layer structures, thin films, plasmonic structures, and low-dimensional materials.^[52,53]

In this review article, we focus on the technical aspects of s-SNOM.^[54] The article is structured as follows. We first give a brief historical overview of the development and evolution of near-field techniques. Then, we discuss the current stage of s-SNOM research by showcasing the latest milestone results published in prestigious journals to provide an overall picture of the capabilities and future potential of s-SNOM. Next, we discuss the technical details and methodological progress both experimentally and theoretically. In conclusion, we present a summary and outlook for the field. Throughout the article, we discuss three key questions in great detail: how do different configurations of s-SNOM work; how can we understand the detected near-field signal; and what is the potential next stage of the technical trend? Previous reviews^[55–60] of s-SNOM have covered the technical progress spanning from the first implementation of SNOMs in the 1970s to research in the 2000s, and specific aspects of s-SNOM methods, such as IR s-SNOM. Here, we briefly introduce the historical developments and focus on the current research stage and beyond. By reviewing publications from the past decade, we discuss the various probing techniques, signal demodulation methods, and progress in analytical and numerical methods for data interpretation.

2. Historical Overview

In 1928, Irish physicist Synge proposed the concept of achieving an optical resolution beyond the diffraction limit^[61] using an opaque metal film with a small aperture placed very close to the sample surface (as illustrated in **Figure 2a**). He envisaged that when the size of the pin hole and the hole-sample distance are much smaller than the wavelength, subdiffraction scattering through the hole can provide super-resolution information. Due to some technical difficulties in his original design, in 1932, he further proposed an alternative scheme in which he suggested the use of a small object as the near-field optical probe (**Figure 2b**)^[62] (O’Keefe^[63] and Wessel^[64] later reinvented the aperture- and scattering-type schemes, respectively, without knowing about Synge’s work). However, Synge’s concepts were never experimentally verified at his time due to the many associated technical challenges. For example, scanning techniques

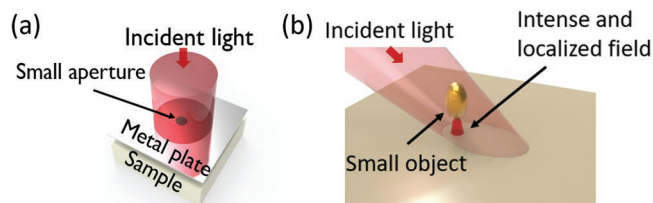


Figure 2. a) Synge’s original concept for overcoming the diffraction limit and achieving an ultrahigh spatial resolution using a small aperture. b) Synge’s second concept with a small subwavelength object as light confiner and scatterer.

such as AFM were not implemented until the 1980s. Additionally, nanotechnology was not as widely explored or applied as it is today. Nevertheless, Synge’s proposal certainly promoted the idea of practically implementing super-resolution methods using the near field.

In the late 1970s and early 1980s, progress in scanning probe technologies with subnanometer precision^[65] eventually led to the experimental fruition of Synge’s ideas, thanks to early pioneers such as Betzig et al., Pohl et al., and Lewis et al.^[66–72] In a 1986 study by the Nobel laureate Betzig et al.,^[68] a line scan across an aluminum grating was performed and yielded a ≈ 150 nm resolution with an incident wavelength of ≈ 500 nm (**Figure 3a**) (aside: readers are encouraged to read Betzig’s Nobel lecture,^[73] in which he eloquently summarizes the quest for subdiffraction resolution from the 1980s to the late 2000s; likewise, his work detailing the concept of near-field optics is still insightful, even for today’s audience.^[69]). In a 2000 study by Hecht et al.,^[74] the measurement of a metal island film achieved a resolution of $\lambda/10$ (≈ 50 nm resolution with a 633 nm incident wavelength) (**Figure 3b**). In both studies, optical contrasts between different materials were clearly observed. Unlike scattering-type near-field systems, near-field instruments in the early days typically used an aperture probe that functioned as a waveguide and subdiffraction emitter,^[74] similar to the original scheme proposed by Synge. Today, aperture-based SNOM is still a popular technique that offers unique advantages, especially those related to visible or ultraviolet illumination.^[75–92] A detailed review of aperture-based SNOM (a-SNOM) can be found in reference.^[74] In principle, a-SNOM can achieve a very high resolution by setting the aperture size to be arbitrarily small. However, in practice, the resolution is limited to $\approx \lambda/10$ due to the waveguide cut-off effect.^[54] Therefore, for mid-IR light, the resolution is on the order of a few hundred nanometers to 1 μm , which in many cases does not meet the desired nanoscale criterion. In the case of THz illumination, the resolution is on the order of tens of micrometers,^[93] at which practical applications in nanoscience become difficult to achieve.

Boosted by the maturity of the AFM technique, intense efforts devoted to developing s-SNOM occurred in the late 1990s. One of these pioneering s-SNOM works was published by Lahrech et al. in 1996.^[94] In their work, they performed s-SNOM imaging of a gold grating and gold surface (**Figure 3c,d**) and observed clear optical contrast at an impressive sub $\lambda/100$ resolution. In the late 1990s and early 2000s, significant instrumental progress, which provided the basis for modern s-SNOM, was made by Knoll et al. and Hillenbrand et al.^[95,96] Unlike a-SNOM, modern s-SNOM typically illuminates a metalized AFM probe with a focused laser beam at an oblique angle of incidence. A metal coating is employed to enhance the scattering efficiency.^[97] The metal-coated tips are usually based on Si cantilevers that are commercially available and economical. The achievable resolution of s-SNOM is only practically limited by the radius of curvature of the tip apex.^[20]

3. Current Stage

The most commonly used contemporary s-SNOM systems are those applicable to the visible and IR frequency ranges using

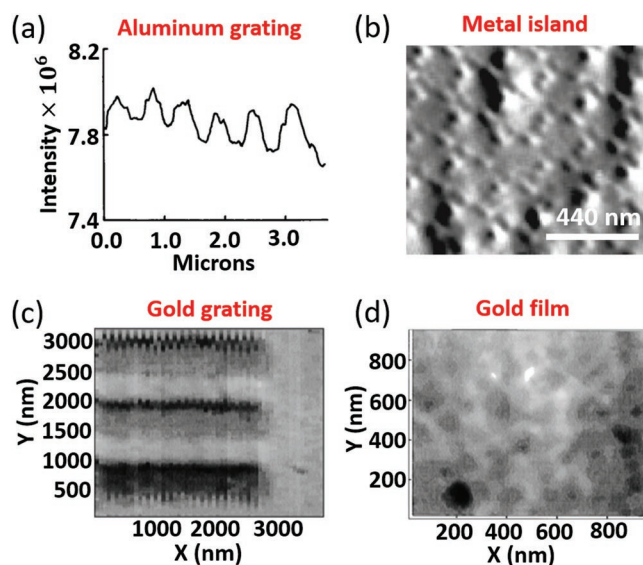


Figure 3. Representative experimental results from early studies using near-field techniques. a) A line scan across an aluminum grating with ≈ 500 nm illumination, reproduced with permission.^[68] Copyright 1986, Elsevier. b) Imaging of a metal island film with 633 nm illumination, reproduced with permission.^[74] Copyright 2000, AIP Publishing. c) Imaging of a gold grating and d) imaging of a gold film surface with 10.6 μ m infrared illumination. (c,d) Reproduced with permission.^[94] Copyright 1996, Optical Society of America (OSA). a,b) are a-SNOM measurements. c,d) s-SNOM measurements.

continuous wave (CW) light sources. With the development of highly stable commercial lasers, such as gaseous, fiber-based, and quantum cascade lasers (QCLs), the typical laser power can now easily reach 0.5–5 mW, as is commonly required in s-SNOM measurements. Additionally, the noise can reach below 100 nV/ $\sqrt{\text{Hz}}$ at ≈ 100 kHz. The result is a promisingly good signal to noise ratio (SNR) for near-field detection, typically above 50 to 1. This SNR is critical for s-SNOM because laser noise is usually the largest limiting factor as the noise of state-of-the-art IR detectors is typically below ≈ 30 nV/ $\sqrt{\text{Hz}}$. In addition to CW lasers, ultrabroadband or tunable light sources, including synchrotron IR radiation and ultrafast fiber or solid-state lasers, have been successfully used for s-SNOM. These sources offer improved temporal and spectral resolutions compared to other source types. The state-of-the-art synchrotron IR source can produce ≈ 1 μ W per wavenumber for a diffraction-limited spot. The result is roughly 1 mW over a 1000 cm^{-1} wide spectral range, which is orders of magnitude higher than that achieved for blackbody radiation sources.

Although s-SNOM is still an emerging field, it has considerable potential to provide new physical insights regarding experimental methods and properties, including nonlocal effects. This is especially true at long wavelengths (e.g., at THz frequencies) because the light can be more tightly confined and nonlocal electron transport significantly contributes to the near-field-accessible sample volume under the tip. Additionally, operating s-SNOM at cryogenic temperatures or in a gaseous environment may aid the quest for investigating low-energy quantum phenomena. By coupling this approach with other imaging techniques, such as focused X-ray diffraction

(nano-XRD) and Raman spectroscopy, s-SNOM can provide a multimodal imaging method with electrons, phonons, and magnetization. In the following sections, we present the basics of such methods and introduce these new branches of s-SNOM in detail. We focus on recent references (mainly around or after 2010) to present the latest progress in this field.

3.1. Prevailing Near-Field Techniques and Major Accomplishments

3.1.1. s-SNOM with CW Light Sources

s-SNOM imaging is best when a monochromatic CW source is used.^[98,99] Most CW lasers in the IR range are capable of providing high output power of up to hundreds of mW and maintain a high level of stability over long periods of time. For example, the hourly power fluctuation of a typical CO₂ laser is usually below 1%. A He-Ne laser can perform much better, with a variation level of less than 0.1%. The high power stability and low RMS noise are crucial for performing long raster scans for high-resolution images.

A typical visible/IR s-SNOM setup is illustrated in **Figure 4**. The incident light is divided by a beamsplitter into a reference arm and a probing arm. The probe beam is focused (within the diffraction limit) with focusing optics, typically a parabolic mirror or a lens, onto the apex of the AFM tip. Light interacts with the tip-sample system and is elastically scattered. The backscattered (or in some cases forward scattered) light follows the same (or different) beam path back to the beam splitter and is eventually collected by the detector. The reference beam is reflected from a flat mirror on a delay stage and interferes with the backscattered light at the detector. The result is the formation of an asymmetric Michelson interferometer. In this approach, both the amplitude and phase information of the scattered light can be obtained, yielding the possibility of extracting local complex dielectric functions of the sample volume under the tip without the Kramers–Kronig relations.

In CW visible/IR s-SNOM research, a wide range of canonical systems have been intensely investigated. The major categories in condensed matter systems include, but are not limited to, mesoscopic phase inhomogeneity in strongly correlated quantum materials (SCQM),^[4,32,100–118] polaritonic wave propagation in plasmonic or dielectric samples, especially low-dimensional materials (graphene, boron nitride, transition metal dichalcogenides, etc.),^[7,119–156] and subwavelength electrodynamic responses from artificial nanostructures.^[5,6,27,29,30,100,131,157–177]

In SCQM^[105,178,179] s-SNOM was first employed to study insulator-metal transitions (IMT) in transition metal oxides. Since most SCQM systems are composed of “bad metals” and “bad insulators,” the optical contrast in a typical near-field image accurately represents the variations in sample permittivity (**Figure 5a**). In a landmark 2007 study by Qazilbash et al., the temperature-induced IMT in vanadium dioxide (VO₂) was directly imaged (**Figure 5b**).^[4] Due to the inhomogeneity in the local dielectric permittivity during the IMT, the local scattering amplitude exhibited distinct contrast. In later studies, unidirectional phase separations were observed in epitaxial VO₂ films grown on TiO₂ substrates with different crystal orientations.^[102,104,106] Due to the distinct strain environment, a variety

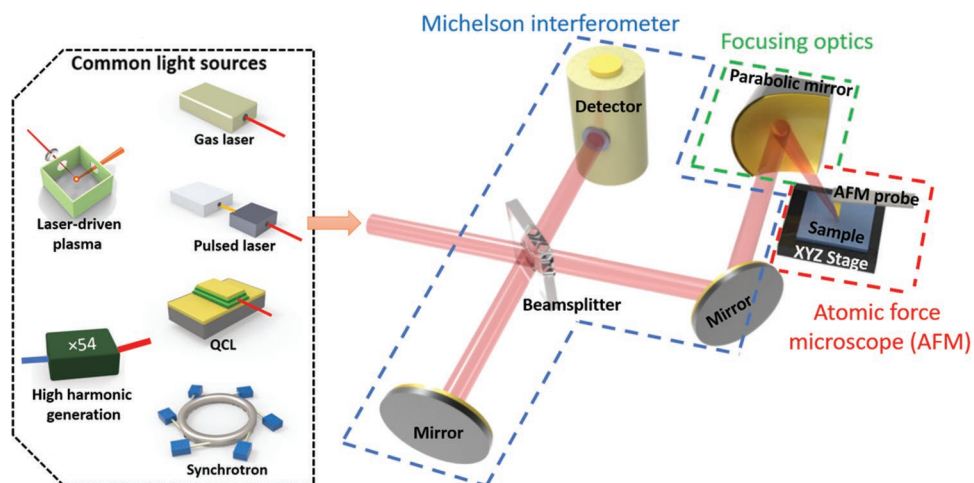


Figure 4. A typical s-SNOM setup with visible or IR light sources. For completeness, a THz CW source, with high-harmonic generation using a microwave, is included.

of pattern formations at elevated temperatures were directly imaged (Figure 5c–e). It is relatively easy to study SCQM with s-SNOM compared to other techniques due to its larger scanning area (up to 100 μm by 100 μm) and wider working temperature range (≈ 10 to ≈ 450 K). A detailed review on this subject was published by Liu et al.^[105] Note that in addition to vanadium compounds, other phase transition materials have been investigated using s-SNOM.^[118] With the development of s-SNOM operating at cryogenic temperatures, more IMT systems, such as organosulfur compounds (Figure 5f)^[116] and rare-earth nickelates (Figure 5g),^[117] have been examined.

Additionally, s-SNOM encompasses a broad range of in-plane momentum due to the light-tip interactions. This property has enabled the direct visualization of surface polaritonic wave propagation, e.g., surface phonon-polariton, plasmon-polariton, and exciton-polariton. In most cases, the AFM tip scatters the incident light and launches a cylindrical polariton

wave of wavelength λ_p . This tip-launched polariton wave can interfere with the boundary-reflected wave (Figure 6a) and form a periodic standing wave of wavelength $\lambda_p/2$. Representative studies by Fei et al., Woessner et al., and Gerber et al. yielded the interference patterns of graphene plasmons shown in Figure 6b–d, respectively.^[6,128,129] In a 2014 study by Dai et al., the interference patterns of surface phonon polariton on a hexagonal boron nitride (hBN) were reported (Figure 6e).^[7] Recently, Hu et al. utilized the interference patterns of waveguide modes to infer the anisotropic dielectric function of MoS_2 (Figure 6f),^[134] and Ma et al. demonstrated the anisotropic polariton propagation process for MoO_3 .^[153] From s-SNOM measurements as discussed above, important polariton properties can be inferred. For example, the dispersion relation can be extracted from the incident frequency and the interference pattern period. Propagation loss can be calculated from the signal amplitude decay.

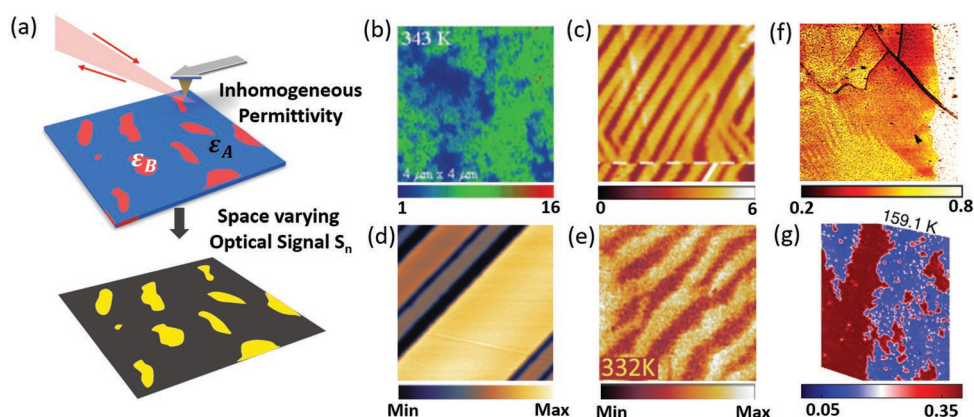


Figure 5. a) Schematic demonstration of the s-SNOM mapping of the local sample permittivity due to phase separation at the nanoscale. ϵ_A and ϵ_B represent two permittivity environments corresponding to different material phases. b–e) Different phase inhomogeneity patterns observed in near-field amplitude images during the temperature-induced IMT phase transition process on VO_2 films grown on different substrates. b) VO_2 on a sapphire substrate, reproduced with permission.^[4] Copyright 2007, The American Association for the Advancement of Science (AAAS). c) VO_2 on $[100]_R \text{TiO}_2$, reproduced with permission.^[104] Copyright 2013, American Physical Society (APS). d) VO_2 on $[110]_R \text{TiO}_2$, reproduced with permission.^[106] Copyright 2014, AIP Publishing. e) VO_2 on $[001]_R \text{TiO}_2$, reproduced with permission.^[102] Copyright 2015, APS. f) Phase inhomogeneity observed on the organosulfur compound BEDT-TTF, reproduced with permission.^[116] Copyright 2018, AAAS. g) Phase inhomogeneity observed on rare-earth nickelate RNiO_3 , reproduced with permission.^[117] Copyright 2018, Springer Nature.

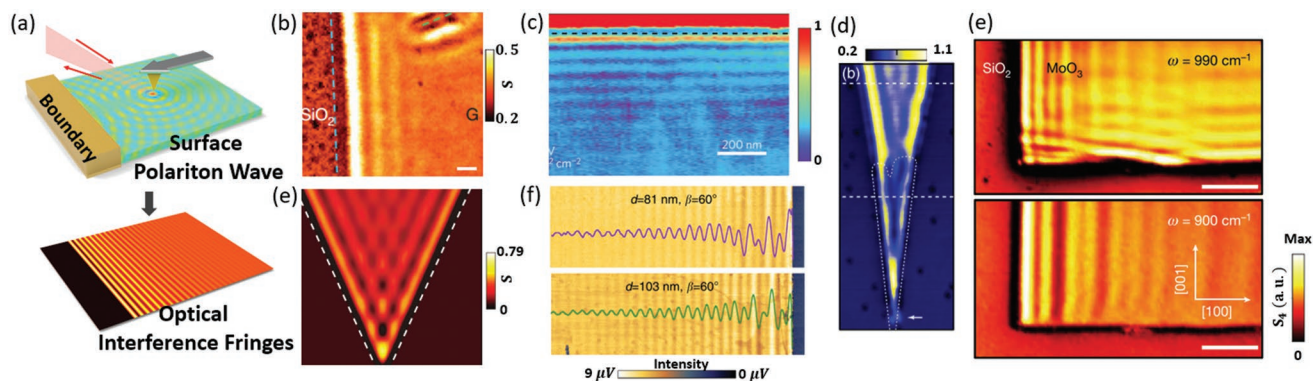


Figure 6. a) Diagrams demonstrating the s-SNOM direct imaging of interference patterns due to propagating polaritonic waves. b–d) Interference of graphene surface plasmons, b) reproduced with permission.^[6] Copyright 2012, Springer Nature; c) reproduced with permission.^[129] Copyright 2014, APS; d) reproduced with permission.^[128] Copyright 2014, Springer Nature. e) Interference pattern of hBN surface phonon polaritons, reproduced with permission.^[7] Copyright 2014, AAAS. f) Interference pattern of MoS₂ waveguide mode, reproduced with permission.^[134] Copyright 2017, Springer Nature. e) Anisotropic polariton propagation on MoO₃, reproduced with permission.^[153] Copyright 2018, Springer Nature.

Another common application of s-SNOM is in studies of plasmonic nanostructures and metamaterials below the scale of a unit cell. The sizes of the unit cells are usually an order of magnitude smaller than the wavelength of interest. Conventionally, the spatial mapping of nanostructure resonances can be indirectly studied by numerical simulations or by far-field measurements. With s-SNOM, different resonance modes can be visualized. Due to the high sensitivity to the local out-of-plane electric fields and charge accumulation, s-SNOM is an ideal tool for visualizing the field and charge distributions induced in plasmonic nanostructures (Figure 7a). For instance, a pioneering study in 2001 by Hillenbrand and Keilmann used s-SNOM to investigate the plasmonic resonance of gold nanoparticles (Figure 7b).^[165] Research interest in this topic

is expected to remain popular in the coming decade. Here, we present results from another three representative studies by Alonso-González et al. and Xu et al. in which nano-disks, bars, and antennas were investigated (Figure 7c–e).^[163,166,169] In metallic nanostructures, localized hot spots form due to the interaction of incident light and confined electrons. Near-field signal is significantly elevated in the hot spots because of enhanced local field and scattering.

Other notable applications of CW visible/IR s-SNOM include studies of the nonlinear and thermal effects in the near field,^[180] the characterization of the sample thickness and optical constants,^[181–185] signal enhancement by manipulating the sample environment,^[186,187] among other related topics. In 2014, Goyadinov et al. demonstrated that the

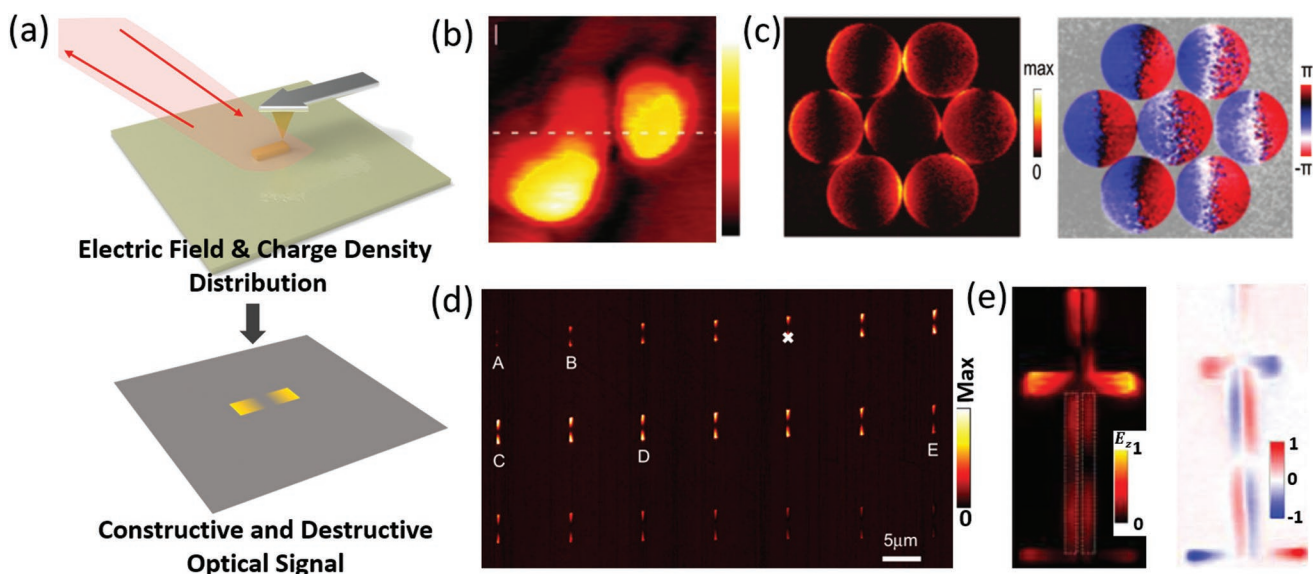


Figure 7. a) Diagrams of the s-SNOM imaging of plasmonic nanostructures. b) Imaging of resonant gold nanoparticles, reproduced with permission.^[165] Copyright 2001, Springer Nature. c) Imaging of a structured disk array, reproduced with permission.^[166] Copyright 2011, American Chemical Society (ACS). d) Investigation of dipolar antennas with different lengths, reproduced with permission.^[163] Copyright 2013, APS. e) Imaging of a folded dipole antenna, reproduced with permission.^[169] Copyright 2016, ACS. The yellow and black color scheme represents the near-field amplitude, and the blue and red color scheme represents phase images.

sample thickness and permittivity can be simultaneously and quantitatively extracted from s-SNOM images demodulated at multiple harmonics of the tip oscillation frequency.^[181] In the following year, Wang et al. showed that it is possible to map the near-field response in both the lateral dimension and the vertical direction, i.e., the near-field confinement in the direction normal to sample surface. This finding provided the ability to map 3D near-field interactions between the tip and sample.^[188,189] Innovative research on CW IR s-SNOM is still rapidly emerging, such as studies involving inter-sub-band transitions in quantum wells and surface states in topological insulators.^[190,191]

3.1.2. s-SNOM in the Time Domain

Ultrafast optics have been widely employed to investigate carrier dynamics at the femtosecond (fs) and nanosecond (ns) time scales.^[192,193] The s-SNOM setup is compatible with conventional pump-probe techniques and various experimental schemes depending on the specific research needs.^[194] An example of the ultrafast pump-probe near-field setup is shown in **Figure 8**.

Ultrafast s-SNOM was pioneered by Wagner et al. in 2014 with seminal works on InAs and exfoliated graphene.^[195,196] By analyzing the area-dependent near-field signal evolution at the ≈ 100 fs scale, the enhanced plasmonic response followed by optical excitation was revealed. This response was attributed to the increase of effective electron temperature following photoexcitation (**Figure 9a**).^[195] Subsequent studies by O'Callahan et al. and Donges et al. used ultrafast IMT dynamics to investigate VO₂ nanocrystals with optical pump/optical probe and near-IR pump/mid-IR probe setups (**Figure 9b,c**), respectively.^[197,198] In a 2014 study by Eisele et al.,^[199] IR-pump multi-THz probe measurements of an InAs nanowire revealed the photoinduced carrier dynamics of the nanowires at a range of 30–40 THz (**Figure 9d**). In a 2016 study by Ni et al.,^[200] an IR-pump IR-probe experiment on graphene yielded the time-dependent plasmon-polariton dispersion properties and showed the time-dependent photodoping effect (**Figure 9e**).

A major goal of ultrafast s-SNOM research is to study photoinduced dynamics without sample size limitations, which has brought nanoconfinement and polaritonic interferometry to the forefront of science. Despite early successes, many

related obstacles must be resolved. For example, the laser repetition rate must be within an appropriate range; if it is too high, the pulse energy will be too small and the accumulated heat will cause serious issues. Conversely, if the rate is too low, the signal detection process will result in a low yield. In addition, a high average power can induce accumulative heating at the tip and result in unstable AFM operation. One possible solution is to use ultrafast s-SNOM systems with repetition rates in the range of a few hundred kilohertz using phase domain sampling techniques.^[201]

3.1.3. s-SNOM for Broadband Nanospectroscopy

Monochromatic illumination produces superior image quality by utilizing the fine linewidth and high power output (watts per wavenumber) in CW lasers. Broadband spectroscopy, on the other hand, delivers point-by-point spectral information over a much broader bandwidth (≈ 200 to ≈ 5000 cm⁻¹). IR spectroscopy is indispensable for probing material vibrational responses. The process of combining spectral measurements in s-SNOM gained popularity in the late 2000s and early 2010s^[11,19,21–23,29,33,47,126,158,160,202–209] with the development of high-power tunable-QCLs and high repetition rate ultrafast fiber-based amplifiers.^[210–212] Synchrotron light sources have also been explored as ultrabroadband sources. Based on Fourier transform infrared spectroscopy (FTIR) techniques that are well established in far-field optics, IR spectroscopy with 10 to 20 nm resolution can be routinely achieved.

The experimental setup of the reference arm differentiates broadband from monochromatic s-SNOM (**Figure 4**). In a broadband s-SNOM experiment, the reference mirror scans over a wider spatial range, and an interferogram (detected light intensity versus optical path difference) is obtained. The complex-valued near-field spectrum is calculated by a Fourier transform of the near-field interferogram. Conversely, a tunable laser system essentially decomposes the experiment into multiple steps involving CW s-SNOM measurements without an interferogram.

Some notable examples of broadband nano-IR experiments are as follows. In a 2012 study by Zhang et al., SiO₂ thin films with different thicknesses on an Si substrate were studied in the frequency domain to assess the accuracy of two different theoretical models. With a combination of QCLs and a CO₂ laser, the authors successfully mapped the spectrum of SiO₂ phonons in the frequency range from 900 to 1300 cm⁻¹ (**Figure 10a**);^[213] in comparison to theoretical calculations, they demonstrated the importance of accounting for the length of the tip shank in theoretical models. In a 2011 study by Fei et al., the hybridization of graphene plasmons and SiO₂ surface phonons was thoroughly investigated with a similar spectroscopy technique (**Figure 10b**).^[47] In a 2014 study by Wagner et al., an IR ultrafast laser was employed as the source for broadband s-SNOM measurements.^[195] Broadband investigations of SCQM can be

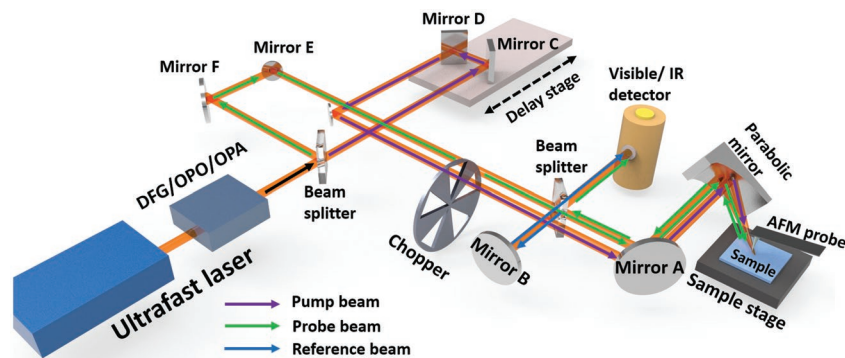


Figure 8. Example of an ultrafast near-field pump-probe spectroscopy setup.

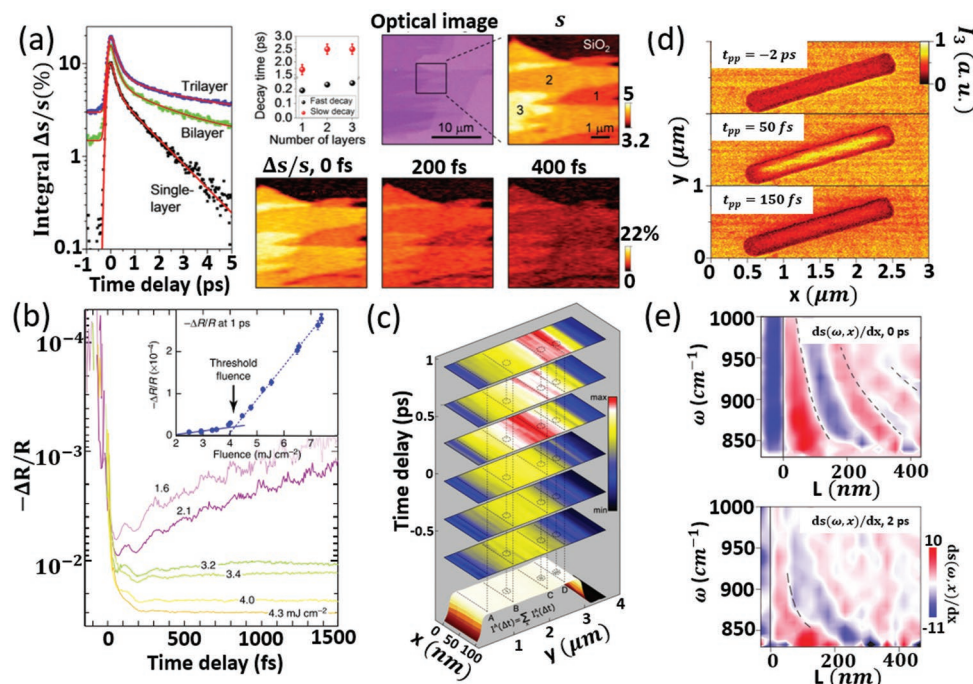


Figure 9. Representative ultrafast s-SNOM studies. a) Near-IR pump/mid-IR probe s-SNOM of graphene, reproduced with permission.^[195] Copyright 2014, ACS. The results show the layer-dependent near-field signal dynamics. b) Optical pump/optical probe of VO₂ nanocrystals, reproduced with permission.^[197] Copyright 2015, Springer Nature. The result shows the transient near-field reflectivity with different pump fluences. c) Near-IR pump/mid-IR probe s-SNOM of VO₂ nanocrystals, reproduced with permission.^[198] Copyright 2016, ACS. The result shows spatiotemporal images of the photoinduced insulator to metal transition. d) IR-pump/multi-THz probe s-SNOM of an InAs nanowire revealing the ultrafast photoinduced carrier dynamics, reproduced with permission.^[199] Copyright 2014, Springer Nature. e) IR-pump/IR-probe s-SNOM of graphene mapping the time-dependent plasmon-polariton dispersion, reproduced with permission.^[200] Copyright 2016, Springer Nature.

performed to infer the correlation between the electron and lattice structures during nanoscale IMTs. For example, in 2015, Liu et al. revealed two different IR active monoclinic phonon modes (M1 and M2) at adjacent locations (subwavelength) on the surface of a single-crystal VO₂ sample (Figure 10c).^[106] In 2014, Hermann et al. characterized the distinct near-field responses of different semiconductors with a broadband synchrotron light source (Figure 10d).^[214] Muller et al. demonstrated the capability to identify the chemical fingerprints of mollusk shells with different compositions (Figure 10e).^[111] Because of its fine spatial resolution, in addition to regular spectroscopy, broadband s-SNOM enables hyperspectral imaging that yields information in both the spatial and frequency domains. Figure 9e is an example of 1D hyperspectral imaging. 2D hyperspectral imaging was demonstrated for a three-component polymer blend by Amenabar et al. in 2017 (Figure 10f).^[208]

Although spectroscopy can be performed with tunable lasers or pulsed lasers, a synchrotron light source (SLS) usually offers a broader simultaneous bandwidth that can greatly enhance the experimental throughput of s-SNOM. An SLS can produce $\approx 1 \mu\text{W}$ per wavenumber for a diffraction-limited spot. The result is $\approx 1 \text{ mW}$ over a 1000 cm^{-1} spectral range, which satisfies the minimum requirement for s-SNOM detection. A number of synchrotron sites provide IR near-field spectroscopy (nano-FTIR) facilities, including the advanced light source (ALS) SINS beamline at Lawrence Berkeley Laboratory (LBL), Berkeley, California, USA; the Metrology Light Source (MLS) in Germany; the Laboratório

Nacional de Luz Síncrotron (LNLS) in Brazil; the ElectroMagnetic Infrared Radiation (EMIRA) facility in Jordan; and the SPring-8 synchrotron site in Japan.^[215–220] These synchrotron light sources can routinely perform IR s-SNOM spectroscopy (also known as nano-FTIR or broadband nano-IR) measurements from below 600 to 2500 cm^{-1} (4 to $15 \mu\text{m}$) with a reliable SNR and a spectral resolution of less than $\approx 8 \text{ cm}^{-1}$.^[9] New possibilities also exist at other national facilities, such as NSLS-II at Brookhaven National Laboratory (BNL), which can, in principle, provide 2 to $100 \mu\text{m}$ wavelength bandwidths for s-SNOM. Another notable technique includes the use of thermal sources as broadband table-top light sources. This process was first demonstrated by Huth et al. using an infrared antenna and later by Lahneman et al. using high-temperature plasma.^[221,222] Recently, Wagner et al. improved both the brightness and SNR of the plasma generation using focused laser techniques.^[223]

3.2. Emerging Techniques and Cutting-Edge Experiments

3.2.1. s-SNOM toward Longer Wavelengths

Based on previous findings, s-SNOM operation in the far-IR and THz frequency ranges deserves its own chapter due to the many associated technical difficulties. As the “THz gap” (a lack of intense sources from ≈ 0.1 to $\approx 10 \text{ THz}$) has been gradually filled in the far field, near-field THz s-SNOM has more

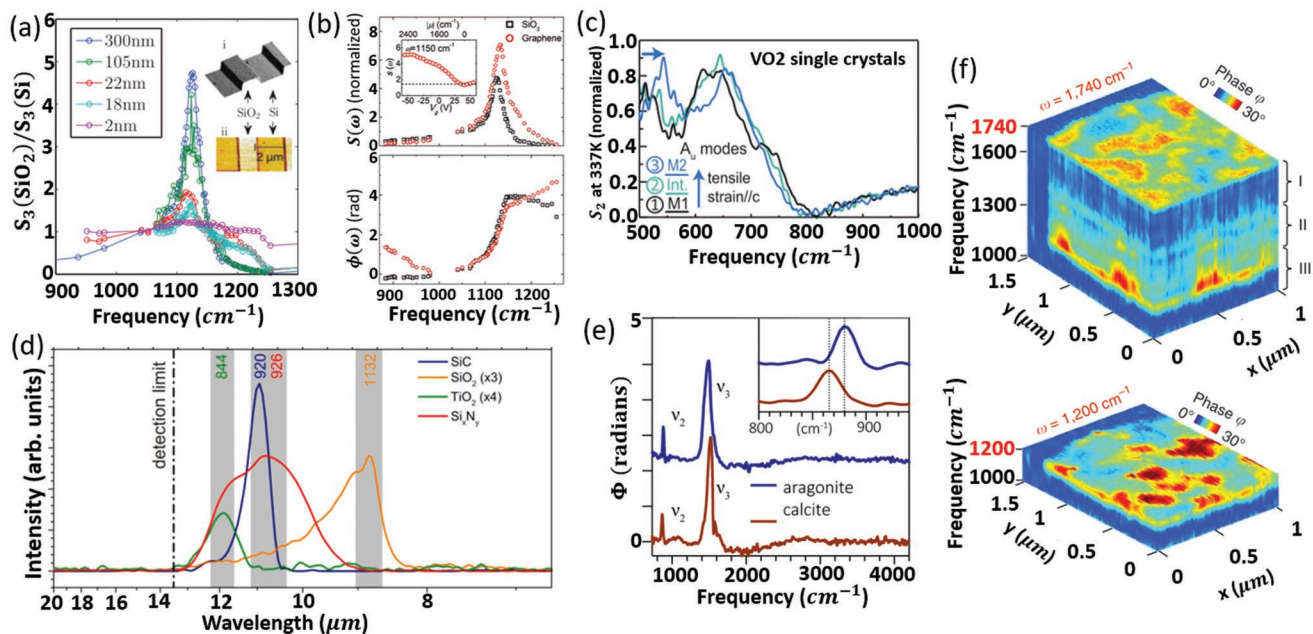


Figure 10. Examples of near-field spectroscopy measurements. a) Near-field spectra of SiO₂ films with different thicknesses, reproduced with permission.^[213] Copyright 2012, APS. b) Near-field spectrum of graphene on SiO₂, reproduced with permission.^[47] Copyright 2011, ACS. c) Location dependent near-field spectrum of single-crystal VO₂ at room temperature, reproduced with permission.^[106] Copyright 2015, APS. d) Near-field spectra of four common semiconductors, reproduced with permission.^[214] Copyright 2014, OSA. e) Near-field spectra of mollusk shells at two different stages (as aragonite and calcite), reproduced with permission.^[11] Copyright 2015, ACS. f) 2D hyperspectral imaging of a three-component polymer blend, reproduced with permission.^[208] Copyright 2017, Springer Nature.

stringent requirements. Of course, challenges and efforts do not come without reward. Due to its low photon energy, THz is ideal for noninvasive diagnosis of biological substances^[224–227] and probing of many low-energy excitations in quantum systems, including phonons, cyclotrons, and the energy gaps in high-*T_c* superconductors and quantum wells.^[228] Accessing the near-field regime is important for many applications in the fields of condensed matter and biophysics, especially when combined with cryogenic conditions, as we will discuss in the next section.

Historically, attempts to generate THz radiation were first performed with frequency mixing,^[229] QCLs,^[230–232] and free-electron lasers. The first series of scattering-based THz near-field experiments were conducted in the mid-2000s.^[233–236] Later, THz waveguide probes were successfully developed in the early 2010s.^[237,238] Higher harmonic signals (*n* ≥ 2) were first experimentally obtained in 2008 by Huber et al. A CW CH₃OH gas laser operating at 2.54 THz was used to image an Si transistor, and the results yielded a quantitative characterization of the local carrier concentration and mobility information at a nanometer-scale resolution (Figure 11a).^[28] In the same year, Ribbeck et al. successfully conducted THz s-SNOM measurements of Si at different doping levels.^[239] In 2012, Jacob et al. used a free-electron laser for THz s-SNOM imaging of InAs quantum dots and successfully observed the contrast induced by the transitions between two confined states belonging to the same band.^[240] At the time of these studies, radiation generated by gaseous lasers and THz QCLs suffered from low emission power or narrow bandwidth issues that limited the corresponding SNR and spectroscopic applications.

THz generated from nonlinear crystals (ZnTe) or the photo-Dember effect (InAs) can, in principle, yield higher instantaneous power (pulse energy divided by the pulse width) and a satisfactory bandwidth.^[239,241,242] However, due to the low repetition rate typically used for pump excitation (e.g., 1 to 10 kHz), an adequate SNR in the near field will require an unbearably long acquisition time. To obtain a high repetition rate, a high SNR THz source must be used. In this case, photoconductive antennas (PCA) have been applied to provide a dynamic range reaching above 80 dB in the 0.2 to 3 THz frequency range.^[243,244] State-of-the-art PCAs can generate ultrashort pulses with a frequency range of up to 15 THz.^[245] With further improvements, PCAs could become a dominant tool for broadband THz s-SNOM.^[246]

As an example, a typical PCA-based THz s-SNOM setup is shown in Figure 12.^[247] To maximize the THz signal, the incident and scattered light components are separated into two different beam paths by removing the beam splitter (this scheme is suitable for IR as well). In practice, two visible guide lasers are often used for the easy alignment of the THz beam. Indium tin oxide (ITO) is effective as a THz mirror and partially transparent to the guide beam. Thus, ITO serves as an ideal dichroic beam splitter for THz and visible light. Since lenses are often avoided for diffraction-limited focusing at THz frequencies, parabolic mirrors are usually required. The scattered light can be collected at the other side and detected at the PCA receiver.

Despite the relative novelty of THz s-SNOM, successful experiments have been performed regularly in recent years. Moon et al. presented a THz s-SNOM imaging study of a gold grating under an Si₃N₄ layer in 2015.^[248] Stinson et al. reported

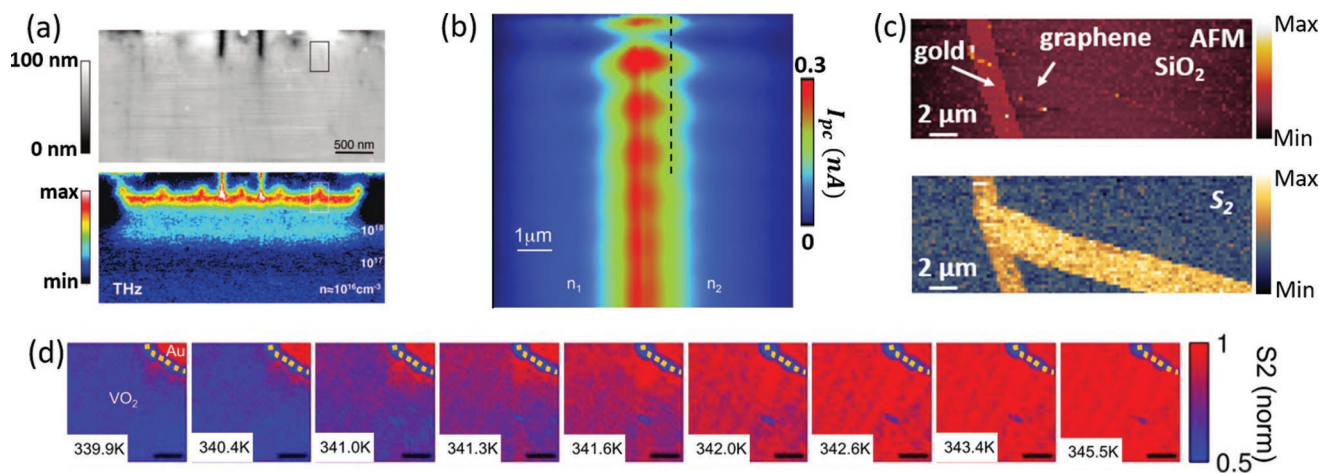


Figure 11. Representative THz s-SNOM studies. a) Top: AFM topography image. Bottom: THz s-SNOM imaging of a transistor device with a gas laser operating at 2.54 THz, reproduced with permission.^[28] Copyright 2008, ACS. Carrier concentration and mobility can be quantitatively identified. b) THz photocurrent imaging of slow plasmons in a split-gate graphene photodetector, reproduced with permission.^[23] Copyright 2016, Springer Nature. c) THz s-SNOM imaging of graphene monolayer with a gold reference and PCA-generated broadband THz illumination, reproduced with permission.^[247] Copyright 2018, ACS. d) THz s-SNOM of the IMT of VO₂ with PCA-generated broadband THz illumination, reproduced with permission.^[249] Copyright 2018, Springer Nature.

the direct observation of the IMT of VO₂ with THz s-SNOM (Figure 11d) in 2018.^[249] In the same year, Zhang et al. observed the high near-field reflectivity of a graphene monolayer (Figure 11c) with a near-field signal comparable to that of noble metals.^[247] Another 2018 study by Liewald et al. proposed an electronic-based s-SNOM setup operating from 0.5 to 0.75 THz based on the high-harmonic generation of microwaves.^[250] Phase-resolved THz s-SNOM using QCL as both a light source and detector was also verified as a potential approach.^[251,252] In addition, recent studies have found various ways to overcome low scattering signal issues with various schemes. For example, in a 2016 study by Alonso-González et al. and a 2017 study by Lundberg et al., THz graphene plasmons were mapped with near-field photocurrent generation (Figure 11b).^[53,253] In a 2017 study by Klarskov et al.,^[254] a THz emission microscopy scheme in which an incident IR beam interacted with the tip-sample system was proposed, and THz emissions due to the nonlinear response were detected. A low repetition rate and high-power THz generation via ZnTe, LiNbO₃, or InAs can, in principle, be achieved in the near-field THz photocurrent and THz emission scenarios because they yield high SNRs. We anticipate this field

becoming a new research frontier filled with exciting physics in upcoming years.

3.2.2. s-SNOM at Low Temperatures and/or in High-Strength Magnetic Fields

A daunting quest in the field of s-SNOM is to perform routine measurements at cryogenic temperatures, namely, cryo-s-SNOM. Although the importance of this task is universally recognized, cryo-SNOM is technically challenging for a number of reasons. For instance, conventional tapping mode AFM does not work easily in high-vacuum and low-temperature environments. Moreover, nine positioners (three for the sample, three for the focusing mirror, and three for the tip) that work independently are required. A cryo-scanner with a reasonably large travel range (since s-SNOM operates at a much larger scanning range than STM) and good radiation shielding to compensate for thermal loss originating from various optical components is needed. The first study of low-temperature s-SNOM was performed by Yang et al., and the study involved the s-SNOM imaging of V₂O₃ during the IMT at ≈200 K (Figure 13a).^[255] In the following year, Döring et al. performed the s-SNOM imaging of the barium titanate ferroelectric domain at ≈222 K (Figure 13b).^[108,256] In 2016, McLeod et al. set a milestone by systematically demonstrating the use of s-SNOM to study SCQM and observed the IMT of V₂O₃ at 160–180 K with high spatial resolution and SNR (Figure 13c).^[3] The low-temperature IMTs of rare-earth nickelates^[117] and organosulfur compounds^[116] have also been investigated with cryo-s-SNOM (Figure 5f,g). Recently, Ni et al. explored the fundamental limits of graphene plasmons with cryo-s-SNOM at 60 K, and long-distance plasmon propagation was observed.^[257]

As cryogenic environments and magnetic degree of freedom often coexist, s-SNOM with a strong magnetic field is another new and exciting research focus. To date, experimental results

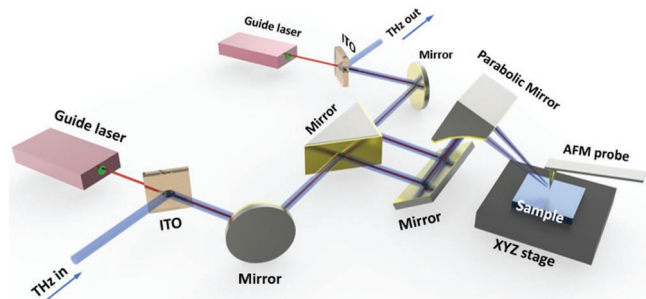


Figure 12. An example of a THz s-SNOM setup, reproduced with permission.^[247] Copyright 2018, ACS.

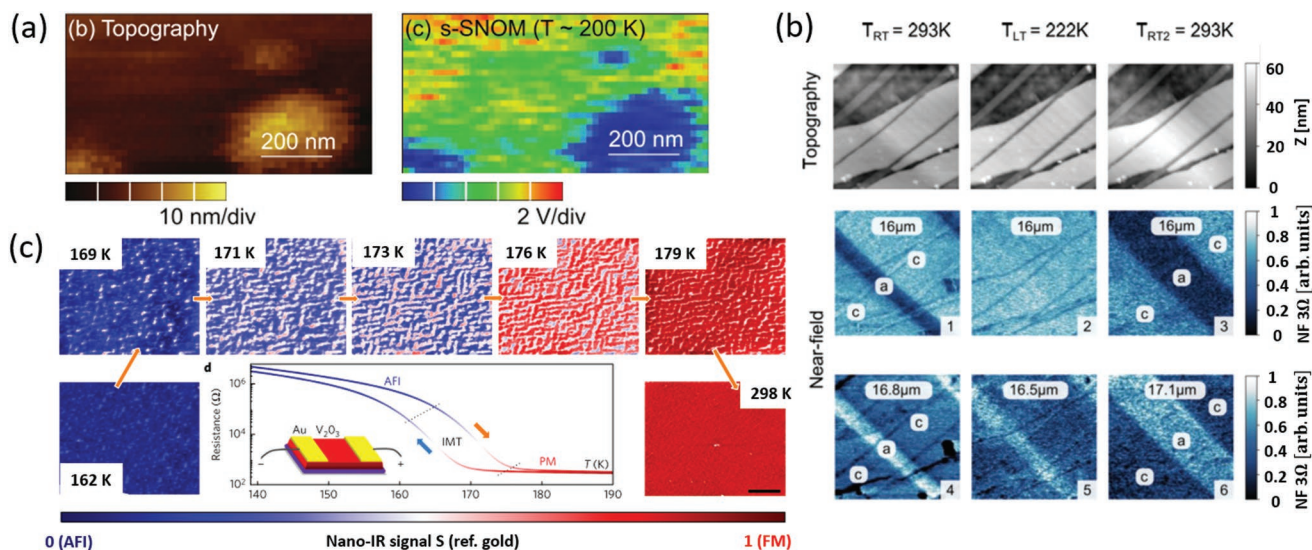


Figure 13. Representative low-temperature s-SNOM studies. a) s-SNOM imaging of V₂O₃ IMT at ≈200 K, reproduced with permission.^[255] Copyright 2013, AIP Publishing. b) s-SNOM imaging of the ferroelectric domains of barium titanate at ≈222 K and room temperature, reproduced with permission.^[108] Copyright 2014, AIP Publishing. c) s-SNOM imaging of V₂O₃ IMT from 169 K to room temperature, reproduced with permission.^[3] Copyright 2016, Springer Nature.

have only been demonstrated with scanning microwave impedance microscopy (sMIM),^[258–261] which relies on electronics instead of optical scanning techniques. Magneto-optical imaging with both a-SNOM and s-SNOM has been demonstrated but requires further exploration.^[262–264]

3.2.3. s-SNOM and Integration with Other Techniques

Inherently, s-SNOM serves as a bridge between far-field electromagnetic propagation and microscopic (near-field) scanning methods. Therefore, this versatile platform can be integrated into many other optical and nonoptical techniques. For example, surface-enhanced Raman spectroscopy (SERS) has gained tremendous popularity over the past couple of decades due to its high sensitivity to molecular vibrations.^[265–267] The concept of combining SERS and s-SNOM has been successfully implemented.

Focused X-ray diffraction (nano-XRD) is an important methodology in crystallography research due to its high spatial resolution, typically at the micrometer scale or lower. Nano-XRD achieves this high resolution by focusing X-rays with a Fresnel zone plate or a Kirpatrick-Baez mirror.^[268,269] State-of-the-art nano-XRD techniques can currently reach a resolution of 30 nm, comparable to the resolution of s-SNOM. Micro- and nano-XRD can be combined with s-SNOM to conveniently and concurrently investigate the optical and structural properties of a sample at the mesoscopic scale. The first such combined system has been developed at the advanced photon source (APS) at Argonne National Laboratory (ANL).

Another potential combination is s-SNOM with scanning thermal microscopy (SThM). SThM measures the thermal properties of a sample, such as the surface temperature and thermal conductivity. The most feasible resolution for commercially available products is close to 50 nm. Coupled with s-SNOM, the

relevant optical and thermal properties can be simultaneously measured. In addition, ultrafast THz STM can be combined with THz cryo-s-SNOM because they share the same essential optics and hardware.

To conclude this section, we present photos of a few tangible s-SNOM systems: a cryo-SNOM (Figure 14a), a synchrotron-based broadband s-SNOM (Figure 14b) and a nano-XRD + s-SNOM (Figure 14c). The complexity of s-SNOM requires a careful examination of the corresponding theory and a detailed understanding of the acquired signals, as will be discussed in the next two sections.

4. Near-Field Signal Detection Schemes

As briefly discussed in the introduction, in s-SNOM experiments, the far-field-detected signal contains genuine near-field information and a strong and undesired background signal associated with the far-field scattering caused by the tip, cantilever, and sample. This background signal creates unwanted artefacts and poses complications when extracting the optical properties of samples. Therefore, a detection scheme that allows for background elimination is necessary in s-SNOM experiments.

To suppress the background signal, the near-field signal is typically modulated with an oscillating AFM probe. In tapping mode, the AFM tip vibrates at a mechanical resonance frequency (Ω) of typically 20–300 kHz depending on the specific cantilever and driving voltage. The near-field signal varies rapidly with the tip-sample distance in a nonlinear fashion, and the background signal varies linearly. Consequently, the demodulated scattering signal at the higher harmonics of the tip tapping frequency (2Ω , 3Ω , etc.) predominantly contains the near-field signal, and the background signal is largely suppressed.

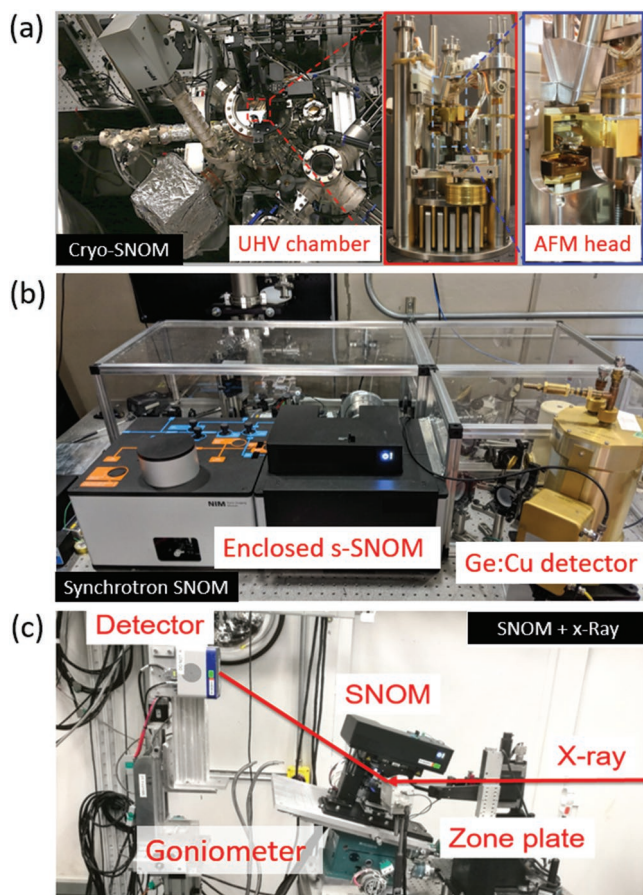


Figure 14. a) A cryo-SNOM currently used in Professor Dimitri Basov's lab at Columbia University. b) Synchrotron-based broadband s-SNOM at ALS, Berkeley. c) A s-SNOM system integrated with a time-resolved X-ray diffraction microscopy beamline by Dr. Haidan Wen at Argonne National Laboratory.

To optimally preserve the near-field signal and reduce the background signal, multiple detection schemes have been developed. In this article, we focus on intensity detection techniques. Electric field detection techniques like electro-optic sampling are viable methods, especially for THz and ultrafast s-SNOM, but are currently less common than other methods. Therefore, we will not discuss these schemes explicitly but simply direct the readers to a paper by Sternbach et al.^[194] Among the various intensity detection techniques, the most implemented are the self-homodyne, homodyne, heterodyne, and pseudo-heterodyne schemes. Here we introduce each method in detail with simplified mathematical treatments and then present their advantages and disadvantages. Detailed mathematical derivations can be found in the respective references. Readers are also encouraged to read the in-depth review article by Dai et al.^[270]

Other less common, yet still successful, detection schemes, such as phase-shifting interferometry^[271] and the synthetic optical holography technique,^[272,273] have also been successfully demonstrated. Due to length constraints, we are not able to discuss these schemes in detail.

4.1. Self-Homodyne Detection (SHD)

In the early stages of s-SNOM, the most common and straightforward detection scheme was SHD, as indicated in **Figure 15a**. The detector only records the signal intensity, which is the squared amplitude of the incident electric field

$$I = (\tilde{E}_n + \tilde{E}_b)(\tilde{E}_n^* + \tilde{E}_b^*) \quad (1)$$

where \tilde{E}_n is the complex near-field scattered electric field and \tilde{E}_b is the complex undesired background. * denotes the complex conjugate. By multiplying the terms and expanding, the following equation can be obtained

$$I = |\tilde{E}_n|^2 + 2|\tilde{E}_n||\tilde{E}_b|\cos(\varphi_n - \varphi_b) + |\tilde{E}_b|^2 \quad (2)$$

The lock-in amplifier demodulates the signal at higher harmonics of the tip tapping frequency. Since \tilde{E}_b varies little with the tip-sample distance, $|\tilde{E}_b|^2$ is mainly removed by filtering after demodulation. Thus, the modulated signal takes the following form

$$I = |\tilde{E}_n|^2 + 2|\tilde{E}_n||\tilde{E}_b|\cos(\varphi_n - \varphi_b) \quad (3)$$

In this case, the detected signal contains a subtle combination of the near-field and background components. Fortunately, in most cases, the second term is much larger than the first term because background scattering is usually orders of magnitude larger than near-field scattering. Thus, the detected signal can be structured based on the near-field signal and enhanced by the background signal. One major drawback of the SHD scheme is that only intensity information is accessible, and phase information is totally lost because φ_b is not a controllable parameter, unlike in more sophisticated detection schemes introduced in the following sections. Furthermore, spatially

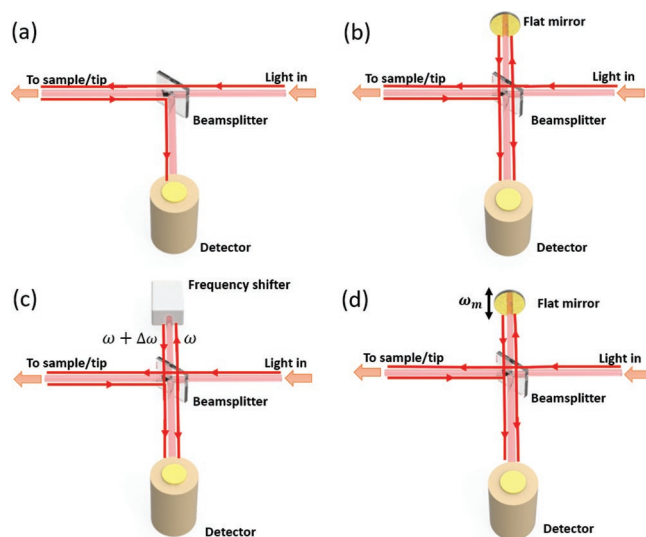


Figure 15. S-SNOM detection schemes. a) Self-homodyne detection. b) Homodyne detection. c) Heterodyne detection. d) Pseudo-heterodyne detection.

varying values of \tilde{E}_b and φ_b could lead to a degree of randomness (artefacts) in the obtained near-field images, making quantitative data interpretation difficult.

4.2. Homodyne Detection (HD)

Currently, SHD is rarely used. Instead, a more advanced detection scheme, HD, is often utilized in s-SNOM setups. Essentially, the homodyne scheme is like the self-homodyne scheme with an added reference arm, such that an asymmetric Michelson interferometer is formed (Figure 15b). With this coherent detection setup, both the amplitude and phase information can be obtained. Based on the detected signal intensity, we have the following equation in this case

$$I = (\tilde{E}_n + \tilde{E}_b + \tilde{E}_r)(\tilde{E}_n^* + \tilde{E}_b^* + \tilde{E}_r^*) \quad (4)$$

where \tilde{E}_r is the reference electric field. By multiplying the terms and expanding, we obtain the following formula

$$I = |\tilde{E}_n|^2 + |\tilde{E}_b|^2 + |\tilde{E}_r|^2 + 2|\tilde{E}_n||\tilde{E}_b|\cos(\varphi_n - \varphi_b) + 2|\tilde{E}_n||\tilde{E}_r|\cos(\varphi_n - \varphi_r) + 2|\tilde{E}_b||\tilde{E}_r|\cos(\varphi_b - \varphi_r) \quad (5)$$

After demodulation by the lock-in amplifier, the $|\tilde{E}_b|^2$, $|\tilde{E}_r|^2$, and $2|\tilde{E}_b||\tilde{E}_r|\cos(\varphi_b - \varphi_r)$ terms are filtered since both \tilde{E}_b and \tilde{E}_r are not modulated by the tip tapping frequency. Therefore, the detected signal becomes

$$I = |\tilde{E}_n|^2 + 2|\tilde{E}_n||\tilde{E}_b|\cos(\varphi_n - \varphi_b) + 2|\tilde{E}_n||\tilde{E}_r|\cos(\varphi_n - \varphi_r) \quad (6)$$

By deliberately increasing the reference beam intensity to a level much higher than that of the probing beam, the first two terms are small compared to the third. In effect, the near-field term scaled by the reference signal is obtained. Since the optical path of the reference beam can be easily adjusted, φ_r is the controlling parameter. Therefore, coherent detection based on both the amplitude and phase is achieved.

Note that in HD, the second term containing the background cannot be totally neglected, especially for reflective samples where \tilde{E}_b is large. In such cases, background artefacts will be present despite the implementation of the demodulation procedure. A common way to minimize these artefacts is to place a reference (thick metal padding, for example) next to the sample. Dividing the signal detected for the sample by the signal detected for the reference can effectively remove spatial variations caused by \tilde{E}_b . Additionally, to obtain the complete information for both the amplitude and phase of the near-field signal, two consecutive scans with the reference mirror at different optical path lengths must be performed. The difference should be $\lambda/8$, or, equivalently, a quarter-wavelength optical path difference corresponding to a 90° phase delay. The real part of the signal can be found when the reference optical path matches the sampling optical path. The imaginary part is identified when the difference between the two optical paths is quarter of the wavelength. This double-pass technique is relatively time-consuming

and requires a high signal stability. However, the homodyne scheme is easy to implement compared to the more sophisticated techniques introduced in the following sections. Therefore, it is still one of the most commonly used detection methods.^[274]

4.3. Heterodyne Detection (HTD)

In principle, the heterodyne detection^[275–277] scheme can suppress the background signal completely. The major difference between heterodyne and homodyne schemes is that the reference beam is frequency shifted from the sampling beam in heterodyne detection and stays the same as that in HD (Figure 15c). In HTD, the reference beam frequency is shifted by a small amount, $\Delta\omega$. This frequency shift is commonly performed with an acousto-optic modulator (AOM). Mathematically, the detected signal is given as follows

$$I = (\tilde{E}_n + \tilde{E}_b + \tilde{E}_r)(\tilde{E}_n^* + \tilde{E}_b^* + \tilde{E}_r^*) \quad (7)$$

However, in the HTD case, \tilde{E}_r denotes the electric field of the frequency-shifted reference. Again, by multiplying the terms and expanding, we obtain the following equation

$$I = |\tilde{E}_n|^2 + |\tilde{E}_b|^2 + |\tilde{E}_r|^2 + 2|\tilde{E}_n||\tilde{E}_b|\cos(\varphi_n - \varphi_b) + 2|\tilde{E}_n||\tilde{E}_r|\cos(\Delta\omega t + \varphi_n - \varphi_r) + 2|\tilde{E}_b||\tilde{E}_r|\cos(\Delta\omega t + \varphi_b - \varphi_r) \quad (8)$$

After demodulation, $|\tilde{E}_b|^2$ and $|\tilde{E}_r|^2$ are essentially removed by filtering due to their time independence. Note that $2|\tilde{E}_b||\tilde{E}_r|\cos(\Delta\omega t + \varphi_b - \varphi_r)$ is associated with frequency $\Delta\omega$, which provides a convenient reference for the optical alignment of the interferometer. The $2|\tilde{E}_n||\tilde{E}_b|\cos(\varphi_n - \varphi_b)$ term is mainly modulated at the tip tapping frequency, Ω . To extract the signal of interest, namely, the $2|\tilde{E}_n||\tilde{E}_r|\cos(\Delta\omega t + \varphi_n - \varphi_r)$ term, we perform demodulation at $n\Omega \pm \Delta\omega$ instead of $n\Omega$. To illustrate the reason for demodulating at $n\Omega \pm \Delta\omega$, we write $2|\tilde{E}_n||\tilde{E}_r|\cos(\Delta\omega t + \varphi_n - \varphi_r)$ as a Fourier series

$$\sum_k A_k |\tilde{E}_n|\cos(k\Omega t)|\tilde{E}_r|\cos(\Delta\omega t + \varphi_n - \varphi_r) \quad (9)$$

Therefore, when demodulated at $n\Omega \pm \Delta\omega$, the amplitude information mostly contains the near-field amplitude enhanced by the reference amplitude. The detected phase information is purely near-field information because the reference phase and the frequency shift are artificially controllable quantities. No uncontrollable background is present.

4.4. Pseudo-Heterodyne Detection (PHD)

As discussed above, in the HTD scheme, the reference beam is usually frequency shifted by an AOM. This method is not universally applicable because commercially available AOMs only operate within a limited spectral range. To overcome this difficulty, the pseudo-heterodyne method was proposed and has been widely implemented.^[278–280] The PHD setup (Figure 15d) is similar to the HD setup. The only difference is that in the

PHD scheme, the reference mirror harmonically vibrates with a small spatial amplitude a at a frequency ω_m much smaller than the AFM probe vibration frequency, Ω . This vibration changes the optical path of the reference arm, causing a phase modulation of the reference beam electric field. This electric field can be written in Fourier series form as follows

$$\tilde{E}_r = \sum_k A_k e^{ik\omega_m t} \quad (10)$$

For this equation, the Fourier coefficients are given by the following formula

$$A_k = AJ_k(a) e^{i\left(\frac{k\pi}{2} + \Delta\phi\right)} \quad (11)$$

where J_k is the k_{th} Bessel function of the first kind and $\Delta\phi$ is the phase difference between the reference beam and sampling beam. Due to this phase modulation of the reference arm, the n_{th} harmonic of the detected signal are split into sidebands at the frequency $n\Omega \pm m\omega_m$. Note that among the sidebands, the signal is successively proportional to the real and imaginary parts of the complex signal. By setting the modulation amplitude a to a specified value, the proportionality of the real and imaginary parts can be equalized. Thus, the PHD scheme allows for the simultaneous measurement of the signal amplitude and phase (or more directly, real and imaginary parts) in one raster scan, yielding excellent time efficiency.

The superior time efficiency and background-free nature of PHD allow this technique to be commonly applied, and it has been used by many researchers pursuing Ph.D. degrees in near-field optics.

5. Analytical Models of Tip Scattering

The complex nature of propagating and nonpropagating waves in near-field detection poses great difficulties to data interpretation. Understanding the scattering pattern of the tip, the important light “mediator” and “scatter” that initiates both the near-field and free space far-field waves, is the first step in obtaining the sample properties encoded in the near-field signal.^[38] In addition, due to the strong coupling of the tip and the sample, each loses their distinct identity, and they become a single entity. Thus, scattering problems involve tip-sample ensembles. The intrinsic length scale for a tip-sample ensemble is on the deep subwavelength scale, which can pose a challenge for calculations based on classical electrodynamic theory. In addition, the tip geometry approximates a cone, which creates a nonintegrable singularity point and length scale mismatch near the tip apex. As a result, analytical modeling or numerical simulation is difficult to perform due to calculation divergence issues and large mesh cell requirements. Nevertheless, with decades of development, the complexity and predictive ability of theoretical and simulation methods have significantly advanced. Various geometries, including spheres, elongated spheroids, hyperboloids, and cones, have been employed to approximate the role of the tip (Figure 16a). In the following section, we introduce various representative models in detail and compare their predictive abilities using the phonon response of SiO₂ as a case study.

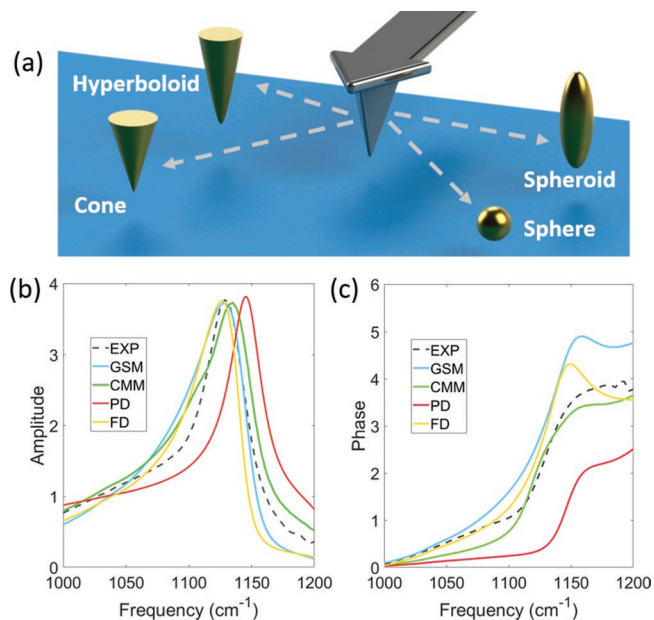


Figure 16. a) Schematic representations of various geometries, including a sphere, elongated spheroid, hyperboloid, and cone, for tip approximation in theoretical models. Third harmonic near-field amplitude b) and phase c) spectra calculated by various models compared to experimentally measured data as a benchmark for model predictability. (b,c) Reproduced with permission.^[303] Copyright 2014, APS. GSM: generalized spectral method; CMM: conformal mapping method; PD: point-dipole mode; FD: finite-dipole mode; and EXP: experimental data.

We also note that the localized field at the vicinity of the tip-sample gap contains a broad momentum distribution. Naively, the dominant momentum is on the order of $1/(\text{tip radius})$. In some cases, especially for certain metals, 2D materials, and thin films, nonlocality will have a significant effect on the momentum; that is, sample properties such as the permittivity and conductivity not only depend on the frequency but also the momentum. The nonlocal effect will be discussed at the end of this section.

5.1. Momentum-Dependent Reflection Coefficient

A straightforward but crude approximation for understanding the s-SNOM signal is the so-called “ r_p approximation,”^[7] with p denoting the p-polarized electric field of the incident wave. In this approximation we completely ignore the geometry of the tip and only account for its presence by considering the momentum-dependent sample response. This response is given by the momentum-dependent p-polarized reflection coefficient.^[281]

$$r_p(\omega, q) = \frac{\epsilon_1 k_0 - \epsilon_0 k_1}{\epsilon_1 k_0 + \epsilon_0 k_1} \quad (12)$$

where ϵ_0 denotes the vacuum permittivity and ϵ_1 denotes the sample permittivity. k_0 and k_1 denote the z-components of the momenta for vacuum and sample. They are given by

$$k_{0,1} = \sqrt{\varepsilon_{1,2} \frac{\omega^2}{c^2} - q^2} \quad (13)$$

where ω is the light frequency and q is the in-plane component of the momentum. Since the confined electric field is evanescent, the imaginary part of $k_{0,1}$ must be a positive nonzero number. Due to tip scattering, the near-field electromagnetic wave has a wide in-plane momentum distribution, with most values being larger than the free space momentum. The q distribution follows a weight function that peaks at roughly $\approx \frac{1}{a}$, where a is the tip apex curvature radius, which typically varies from 10 to 100 nm. Since $q \gg \frac{\omega}{c}$ in most cases, r_p can be further approximated by a q -independent function obtained found by taking the limit as $q \rightarrow \infty$

$$r_p(\omega) = \frac{\varepsilon_1 - \varepsilon_0}{\varepsilon_1 + \varepsilon_0} = \frac{\varepsilon_1 - 1}{\varepsilon_1 + 1} \quad (14)$$

We must stress that the r_p approximation only provides a simple understanding of the physical process in a near-field experiment and is not expected to provide any quantitative predictability. However, the importance of the approximation should not be overlooked as it functions as a stepping stone for future developments of more complicated models. Several studies, mostly involving 2D materials, have been successfully interpreted based on this simple approach.^[7,47,282]

5.2. Point-Dipole Model

Many theoretical investigations of the behavior of a polarized particle above an infinite plane have been conducted since over half a century ago.^[281,283–288] In the late 1990s, a point-dipole model was applied to s-SNOM for data interpretation.^[289] In this model, the tip was approximated as a polarized sphere and then as a point dipole with the same polarizability.^[54,290,291] This model, both in its original version and modified versions, has successfully produced results that agree with the experimental data, at least at a qualitative level.^[47,213,292–294] With this approximation, the problem at hand essentially becomes a light scattering problem involving a small particle (AFM tip) above an infinite half space (sample). A rigorous mathematical treatment of this problem can be found in reference.^[281,295,296] Here, we only briefly discuss the concept of the model without providing the details. Additionally, we only present the simplest version of the point-dipole model, in which 1) the sample is treated as an isotropic infinite half space, 2) only the vertical component of the electric field is considered, 3) a quasi-electrostatic approximation is imposed, and 4) the retardation effect is ignored. Note that more complex versions of the point-dipole model have been developed over the years, as have the point-dipole model for anisotropic samples^[297] and the point-dipole model for multilayer samples.^[186] Retardation and multiple scattering effects have also been considered.^[298] Furthermore, beyond the dipole approximation, the multipole moments of the probe have been taken into consideration.^[298,299] In 2011, a modified dipole model for THz s-SNOM analysis was proposed by Moon et al.^[293] All these modifications have made the point-dipole

model more generic and yielded improved consistency with experimental results.

In its simplest form, the AFM tip can be approximated as a polarized sphere with dielectric constant ε_t and radius a located at position $(0, 0, z + a)$. In most cases, ε_t is assumed to be constant at the frequency of interest. The polarizability of the sphere is given by

$$\alpha = 4\pi a^3 \frac{\varepsilon_t - \varepsilon_i}{\varepsilon_t + 2\varepsilon_i} \quad (15)$$

where ε_i is the dielectric constant of the surrounding medium. In our case, the tip is typically in an ambient environment, so we can take $\varepsilon_i = 1$ and

$$\alpha = 4\pi a^3 \frac{\varepsilon_t - 1}{\varepsilon_t + 2} \quad (16)$$

To further simplify the mathematics, we can replace the sphere with a point dipole of equal strength. Now, we consider the following sample: the infinite half space $z < 0$. The classical image method can be applied here. Equivalently, consider an image dipole with polarizability $\alpha\beta$ located at $(0, 0, -(a+z))$, where $\beta = \frac{\varepsilon_s - 1}{\varepsilon_s + 1}$ is the dielectric surface response function (as in the r_p model discussed in the previous subsection) and ε_s is the dielectric constant of the sample.

The interaction between the tip dipole and the sample dipole is reflected in the near-field response observed in s-SNOM experiments. Using the Maxwell equations with an electrostatic limit, we conclude that the effective polarizability of the tip-sample system is given by

$$\alpha_{\text{eff}} = \frac{\alpha(1+\beta)}{1 - \alpha\beta/(16\pi(a+z)^3)} \quad (17)$$

The scattered field is proportional to the polarizability. Finally, to compare this result with the experimental data, it is crucial to demodulate α_{eff} at higher harmonics of the probe oscillation frequency, i.e.

$$S_n \sim \int_0^T \alpha_{\text{eff}}(z(t), \omega) e^{in\Omega t} dt \quad (18)$$

where S_n represents the n th harmonic of the near-field signal, Ω is the tip oscillation frequency and $T = \frac{2\pi}{\Omega}$ is the tip oscillation period.

5.3. Finite-Dipole Model

Despite its simplicity, the point-dipole model provides relatively poor quantitative predictions for slightly more complex systems, such as those with strongly resonant samples. This decrease in performance is mainly due to the inaccurate approximation of the tip geometry. Specifically, the elongated shape of the tip shank is ignored, which leads to the underestimation of the antenna effect. To further advance the model, an elongated spheroid-shaped tip was considered in the late 2000s.^[300] Here, we briefly discuss some important results

of the finite-dipole model. A more detailed derivation can be found in reference.^[300]

Based on a previous study of a conducting prolate spheroid under illumination,^[301] it is known that only localized charges near the end of the spheroid must be considered to obtain a good approximation of the physical situation. The fraction of the localized charge to the induced total charge g depends on the tip-sample distance but becomes relatively constant as it approaches 0.7. Again, using the image method, we conclude that the effective polarizability of the spheroid is given by

$$\alpha_{\text{eff}} = R^2 L \frac{\frac{2L}{R} + \ln \frac{R}{4eL}}{\ln \frac{4L}{e^2}} \left(2 + \frac{\beta \left(g - \frac{R+H}{L} \right) \ln \frac{4L}{4H+3R}}{\ln \frac{4L}{R} - \beta \left(g - \frac{3R+4H}{4L} \right) \ln \frac{2L}{2H+R}} \right) \quad (19)$$

where R is the tip apex radius, L is the tip length, H is the tip-sample distance, g is roughly 0.7, and $\beta = \frac{\epsilon_s - 1}{\epsilon_s + 1}$, as in the point dipole model.

Due to the elongated length of the spheroid, the role of the tip as a light-confining antenna is well reproduced. Therefore, this model yields good quantitative consistency with the experimental data.^[302]

5.4. Models beyond Closed-Form Solutions

In both the point-dipole and finite-dipole models, an analytical expression of α_{eff} can be found. Beyond these closed-form solutions, mathematically rigorous treatments of the tip with spheroid- or hyperboloid-related shapes have been further considered to improve the accuracy of the predictions. Mathematical details are omitted in this article due to their complexity but can be found in.^[303,304] With those treatments, superior predictive ability can be achieved. It is instructive to note that, as pointed out by Yang et al. in reference,^[304] the point-dipole model and finite-dipole model attempt to approximate a continuous charge distribution as a point source. As a consequence, only the lowest order localized surface mode is preserved, and higher order modes are ignored. This issue can lead to quantitative inaccuracies, especially when the sample has strong electromagnetic resonance.

A more intriguing and realistic tip geometry, namely a cone, has never been analytically considered until recently because of the nonintegrable singularity at the tip. This difficulty has been circumvented by the conformal mapping method. This pioneering method has displayed excellent quantitative agreement with experiments and is temporally efficient; notably, the calculation can be done in seconds, which is fast even when compared to previously introduced analytical models. The mathematical details are omitted here but can be found in reference.^[305]

As a benchmark for the performance of the models introduced above, we performed calculations of the near-field spectra in 1000–1200 cm^{-1} frequency range for the representative material SiO_2 . SiO_2 is a great candidate for experiments because SiO_2 exhibits a well-known phonon-polariton mode at $\approx 1130 \text{ cm}^{-1}$ that displays a distinct response in the spectrum.

Calculations based on the point-dipole model (PD), finite-dipole model (FD), generalized spectral method (GSM), and conformal mapping method (CMM), as well as an experimental (EXP) measurement, are shown in Figure 16b,c. The variations in the predictive abilities of these models, especially for the phase spectra, are evident.

5.5. Numerical Methods

Aside from analytical methods, full-wave simulations using various algorithms, including finite element methods, finite-difference time-domain methods, and other methods, can be employed to model a scattered signal. Commercially available solvers such as CST Microwave STUDIO, Lumerical FDTD, and COMSOL MULTIPHYSICS provide convenient modeling platforms and effective calculation algorithms. The geometry of the tip and sample can be represented with few approximations. Several studies have employed a signal demodulation procedure in simulations and obtained quantitatively consistent results.^[306–308] More straightforward methods that do not consider the tip modulation have also been implemented by simply considering the electric field intensity between the tip and the sample proportional to the near-field signal. Due to its time efficiency, using the electric field intensity near the sample surface to approximate the near-field signal is also a common practice, especially in studies of plasmonic nanostructures.^[127,159,162–164,294,309–311]

5.6. Nonlocality in s-SNOM

In previous discussions, we only explicitly considered the frequency dependence of the sample permittivity. It is important to note that in general, there is a momentum dependence as well (nonlocality). Here, we only briefly discuss this nonlocal effect, which deserves more attention in the future.

There are three crucial relevant length scales in an s-SNOM measurement: the free space wavelength λ , the tip apex radius a , and the particle or quasiparticle mean free path of the sample material d . Correspondingly, there are three relevant momentum scales: the free space light momentum $q_1 = \frac{\omega}{c} = \frac{2\pi}{\lambda}$, confined (near-field) wave momentum $q_2 \approx \frac{1}{a}$, and particle or quasiparticle momentum $q_3 = \frac{\omega}{v_F} \sim \frac{2\pi}{d}$, where v_F is the Fermi velocity of the material. Typically, the condition $q_1 \ll q_2 \ll q_3$ is met because $d \leq a \leq \lambda$. Under this condition, the quasistatic treatment of the tip-sample interaction (no retardation) and local approximation of the optical constant of the sample ($\epsilon(\omega, \mathbf{q}) \rightarrow \epsilon(\omega)$) can be justified. However, in some cases in which ω is small, e.g., with THz or microwave illumination, q_2 can become comparable to or even larger than q_3 . Thus, the local approximation is invalid. To account for this nonlocality, the momentum dependence of the optical constant $\epsilon(\omega, \mathbf{q})$ must be carefully addressed. To date, this intrinsic nonlocality has only been observed and theoretically understood within s-SNOM experiments involving low-dimensional materials such as graphene^[6,53] and plasmonic nanostructures made of noble metals.^[161]

6. Others

Since s-SNOM is an ever-growing field, it is impractical to cover all the relevant aspects of related research in this short review. Many near-field-related experiments are performed in various ways that differ from the methods introduced in this article. Here, we note only a few novel concepts and approaches related to this research frontier.

- 1) Using an intense pulsed laser source, the AFM-IR technique does not detect the scattered light. Instead, it directly probes the oscillation of the AFM tip in contact mode to yield the IR absorption spectrum via the photothermal expansion of the sample surface.^[312–325] This concept was recently applied for operation in peak-force mode to enable simultaneous nanoscale mechanical mapping.^[326,327]
- 2) Operating s-SNOM in peak-force mode (PF-SNOM) is another innovative technique.^[328] In this method, the mechanical properties of the sample can be simultaneously obtained in parallel to the optical information.
- 3) Komiyama et al. recently proposed an interesting method of investigating the thermal radiation of a sample with s-SNOM.^[329] In their work, a passive imaging technique was proposed in which the thermal evanescent waves from the

sample surface directly provided near-field interactions with the tip and eventually scattered into the far-field. Another recent work by Weng et al. proposed an s-SNOM-based method of imaging nonlocal electron energy dissipation by measuring the local current fluctuations generated by nonequilibrium electrons.^[330]

- 4) Furthermore, the current spatial resolution of s-SNOM is predominantly limited by the curvature radius of the tip apex. A new method to improve the resolution was recently proposed without making the curvature sharper. Greener et al. demonstrated that by using two excitation sources with different frequencies instead of one, the spatial resolution can be greatly enhanced.^[331] Future research is still needed to advance this concept. In addition, since the tip plays such a significant role in s-SNOM, a number of studies that focused on improving the tip scattering efficiency and the near-field signal level have been performed.^[49,332–336]

7. Summary and Outlook

The deterministic characterization of optical properties over a broad spectral range at a nanometer resolution is an immense challenge. This review merely scratched the surface of this

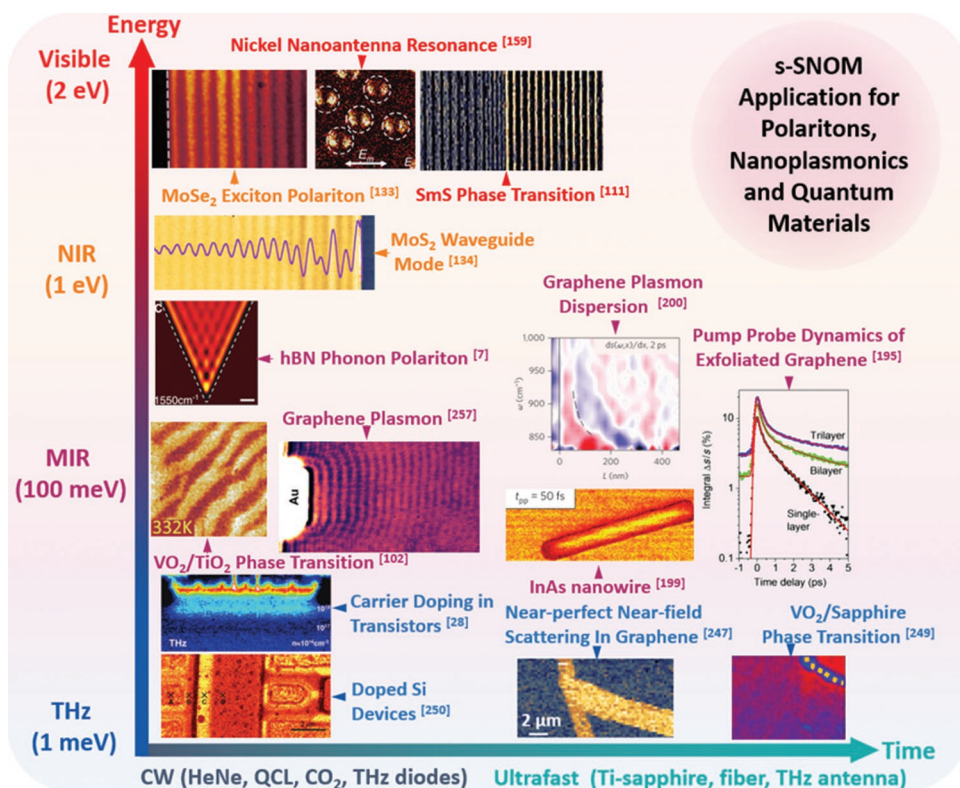


Figure 17. Summary of the applications of s-SNOM showing some iconic phenomena at the characteristic frequency and time scales. Reproduced with permission.^[133] Copyright 2017, Springer Nature. Reproduced with permission.^[159] Copyright 2011, John Wiley and Sons. Reproduced with permission.^[111] Copyright 2017, Springer Nature. Reproduced with permission.^[134] Copyright 2017, Springer Nature. Reproduced with permission.^[7] Copyright 2014, AAAS. Reproduced with permission.^[102] Copyright 2013, APS. Reproduced with permission.^[257] Copyright 2018, Springer Nature. Reproduced with permission.^[28] Copyright 2008, ACS. Reproduced with permission.^[250] Copyright 2018, OSA. Reproduced with permission.^[200] Copyright 2016, Springer Nature. Reproduced with permission.^[199] Copyright 2014, Springer Nature. Reproduced with permission.^[195] Copyright 2014, ACS. Reproduced with permission.^[247] Copyright 2018, ACS. Reproduced with permission.^[249] Copyright 2018, Springer Nature.

subject by introducing the basics of detection and data interpretation schemes. The continual desire for finer spatial resolutions may eventually force researchers to redefine the use of macroscopic optical parameters based on the validity of the concept of quasiparticles, e.g., the semiclassical treatment of the dielectric constant. The fact that the tip is an essential part of the system provides both obstacles and opportunities, whereas the passive role played by the tip may very well be reversed in the future. For instance, when both the tip and sample become quantum objects where discrete optical states can exist, quantum entanglement between the tip and sample may occur. Reverse quantum actions, quantum information storage, and causality may then become important research topics in the future.^[97,337,338]

Before near-field quantum optics are explored at such levels, many daunting tasks must be accomplished. One of the most attainable goals in the near future is the measurement of the momentum-dependent nonlocality of electrons at cryogenic temperatures with low-energy photoexcitation. Investigations with precise control of the tip modality, further improvements in the theoretical modeling of sample inhomogeneity and anisotropy, and full consideration of the local and nonlocal magnetic, thermal, and aerodynamic environments must be performed in the future.

In conclusion, we list a summary chart showcasing some iconic phenomena and their characteristic frequency and time scales in **Figure 17**. A few of the phenomena are unique to near-field characterizations, but most benefit from other means of measurements as well. By coupling s-SNOM with ultrafast optics, nano-XRD, Raman, and perhaps STM, the next generation of multimodal imaging tools for material characterization is quickly emerging. Such tools are not only applicable in the field of condensed matter physics but also in broader communities, including chemistry, biology, and various fields of engineering. The immense and increasing amount of imaging data available will benefit the creation of efficient platforms to display, organize and compare results among different research groups. Interactive big databases, systematic analysis tools, and “deep learning” image processing methods can greatly advance the field as a whole. Overall, s-SNOM research is still in its adolescent phase, and the subsequent progression to a mature field will surely make it an indispensable tool in the future exploration of the nanoworld.

Acknowledgements

The authors thank Alexander S. McLeod, Wenjie Wang (Ithatron Optics), Andrea Huber (Neaspec, Inc.), G. Lawrence Carr, Hans A. Bechtel, Michael Martin, Haidan Wen, S. T. Chui, and Gregory O. Andreev for their helpful discussions. Q.D. and D.H. thank the support from the National Basic Key Research Program of China (No. 2015CB9324000) and the National Natural Science Foundation of China (No. 11704085). The work at Columbia University on correlated oxides is supported by DOE-BES-DE-SC-0012375. Research at Columbia on graphene is supported by DOE-BES DE-SC0018426. The development of cryogenic nanoimaging at Columbia is supported by ONR-N000014-18-1-2722 and AFOSR: FA9550-15-1-0478. The development of multimodal and multiscale imaging methods at Columbia is supported as part of Programmable Quantum Materials, an Energy Frontier Research Center funded by the U.S. Department of Energy (DOE), Office of Science, Basic Energy

Sciences (BES), under award DE-SC0019443.” The research in ultrafast nano-optical methods is funded by DOE-BES-DE-SC0018218. D.N.B. is a Gordon and Betty Moore Foundation investigator under EPIQS Initiative Grant GBMF4533.

Conflict of Interest

The authors declare no conflict of interest.

Keywords

infrared, near-field microscope, near-field optics, SNOM, s-SNOM, terahertz

Received: July 25, 2018

Revised: February 27, 2019

Published online:

- [1] E. Abbe, *Arch. Mikrosk. An'at.* **1873**, 9, 413.
- [2] T. Taubner, R. Hillenbrand, F. Keilmann, *J. Microsc.* **2003**, 210, 311.
- [3] A. S. McLeod, E. van Heumen, J. G. Ramirez, S. Wang, T. Saerbeck, S. Guenon, M. Goldflam, L. Anderegg, P. Kelly, A. Mueller, M. K. Liu, I. K. Schuller, D. N. Basov, *Nat. Phys.* **2016**, 13, 80.
- [4] M. M. Qazilbash, M. Brehm, B.-G. Chae, P.-C. Ho, G. O. Andreev, B.-J. Kim, S. J. Yun, A. V. Balatsky, M. B. Maple, F. Keilmann, H.-T. Kim, D. N. Basov, *Science* **2007**, 318, 1750.
- [5] J. Chen, M. Badioli, P. Alonso-González, S. Thongrattanasiri, F. Huth, J. Osmond, M. Spasenović, A. Centeno, A. Pesquera, P. Godignon, A. Zurutuza Elorza, N. Camara, F. J. G. de Abajo, R. Hillenbrand, F. H. L. Koppens, *Nature* **2012**, 487, 77.
- [6] Z. Fei, A. S. Rodin, G. O. Andreev, W. Bao, A. S. McLeod, M. Wagner, L. M. Zhang, Z. Zhao, M. Thiemens, G. Dominguez, M. M. Fogler, A. H. C. Neto, C. N. Lau, F. Keilmann, D. N. Basov, *Nature* **2012**, 487, 82.
- [7] S. Dai, Z. Fei, Q. Ma, A. S. Rodin, M. Wagner, A. S. McLeod, M. K. Liu, W. Gannett, W. Regan, K. Watanabe, T. Taniguchi, M. Thiemens, G. Dominguez, A. H. C. Neto, A. Zettl, F. Keilmann, P. Jarillo-Herrero, M. M. Fogler, D. N. Basov, *Science* **2014**, 343, 1125.
- [8] B. Pollard, E. A. Muller, K. Hinrichs, M. B. Raschke, *Nat. Commun.* **2014**, 5, 3587.
- [9] H. A. Bechtel, E. A. Muller, R. L. Olmon, M. C. Martin, M. B. Raschke, *Proc. Natl. Acad. Sci. USA* **2014**, 111, 7191.
- [10] A. Bouhelier, *Microsc. Res. Tech.* **2006**, 69, 563.
- [11] E. A. Muller, B. Pollard, M. B. Raschke, *J. Phys. Chem. Lett.* **2015**, 6, 1275.
- [12] B. Kästner, C. M. Johnson, P. Hermann, M. Kruskopf, K. Pierz, A. Hoehl, A. Hornemann, G. Ulrich, J. Fehmel, P. Patoka, E. Rühl, G. Ulm, *ACS Omega* **2018**, 3, 4141.
- [13] M. Filimon, I. Kopf, F. Ballout, D. A. Schmidt, E. Bründermann, J. Rühle, S. Santer, M. Havenith, *Soft Matter* **2010**, 6, 3764.
- [14] V. Stanic, F. C. B. Maia, R. de Oliveira Freitas, F. E. Montoro, K. Evans-Lutterodt, *Nanoscale* **2018**, 10, 14245.
- [15] T. Craig, A. D. Smith, G. M. Holder, J. Ingham, C. I. Smith, A. Varro, D. M. Pritchard, S. D. Barrett, D. S. Martin, P. Harrison, A. Wolski, A. Cricenti, M. Luce, M. Surman, S. Chattopadhyay, P. Weightman, M. R. F. Siggel-King, *Phys. Status Solidi B* **2018**, 255, 1700518.
- [16] D. Perez-Guaita, K. Kochan, M. Batty, C. Doerig, J. Garcia-Bustos, S. Espinoza, D. McNaughton, P. Heraud, B. R. Wood, *Anal. Chem.* **2018**, 90, 3140.

- [17] N. Qin, S. Zhang, J. Jiang, S. G. Corder, Z. Qian, Z. Zhou, W. Lee, K. Liu, X. Wang, X. Li, Z. Shi, Y. Mao, H. A. Bechtel, M. C. Martin, X. Xia, B. Marelli, D. L. Kaplan, F. G. Omenetto, M. Liu, T. H. Tao, *Nat. Commun.* **2016**, *7*, 13079.
- [18] S. Berweger, D. M. Nguyen, E. A. Muller, H. A. Bechtel, T. T. Perkins, M. B. Raschke, *J. Am. Chem. Soc.* **2013**, *135*, 18292.
- [19] M. Paulite, Z. Fakhraai, I. T. S. Li, N. Gunari, A. E. Tanur, G. C. Walker, *J. Am. Chem. Soc.* **2011**, *133*, 7376.
- [20] M. Brehm, T. Taubner, R. Hillenbrand, F. Keilmann, *Nano Lett.* **2006**, *6*, 1307.
- [21] S. Amarie, P. Zaslansky, Y. Kajihara, E. Griesshaber, W. W. Schmahl, F. Keilmann, *Beilstein J. Nanotechnol.* **2012**, *3*, 312.
- [22] I. Amenabar, S. Poly, W. Nuansing, E. H. Hubrich, A. A. Goyadinov, F. Huth, R. Krutokhvostov, L. Zhang, M. Knez, J. Heberle, A. M. Bittner, R. Hillenbrand, *Nat. Commun.* **2013**, *4*, 1.
- [23] O. Khatib, J. D. Wood, A. S. McLeod, M. D. Goldflam, M. Wagner, G. L. Damhorst, J. C. Koepke, G. P. Doidge, A. Rangarajan, R. Bashir, E. Pop, J. W. Lyding, M. H. Thiemens, F. Keilmann, D. N. Basov, *ACS Nano* **2015**, *9*, 7968.
- [24] J. Jiang, S. Zhang, Z. Qian, N. Qin, W. Song, L. Sun, Z. Zhou, Z. Shi, L. Chen, X. Li, Y. Mao, D. L. Kaplan, S. N. Gilbert Corder, X. Chen, M. Liu, F. G. Omenetto, X. Xia, T. H. Tao, *Adv. Mater.* **2018**, *30*, 1705919.
- [25] I. Kopf, C. Grunwald, E. Bründermann, L. Casalis, G. Scoles, M. Havenith, *J. Phys. Chem. C* **2010**, *114*, 1306.
- [26] B. J. Bohn, M. Schnell, M. A. Kats, F. Aieta, R. Hillenbrand, F. Capasso, *Nano Lett.* **2015**, *15*, 3851.
- [27] M. Schnell, P. Sarriugarte, T. Neuman, A. B. Khanikaev, G. Shvets, J. Aizpurua, R. Hillenbrand, *Nano Lett.* **2016**, *16*, 663.
- [28] A. J. Huber, F. Keilmann, J. Wittborn, J. Aizpurua, R. Hillenbrand, *Nano Lett.* **2008**, *8*, 3766.
- [29] A. J. Huber, J. Wittborn, R. Hillenbrand, *Nanotechnology* **2010**, *21*, 235702.
- [30] A. J. Huber, D. Kazantsev, F. Keilmann, J. Wittborn, R. Hillenbrand, *Adv. Mater.* **2007**, *19*, 2209.
- [31] A. Gozar, N. E. Litombe, J. E. Hoffman, I. Božović, *Nano Lett.* **2017**, *17*, 1582.
- [32] J. Rensberg, S. Zhang, Y. Zhou, A. S. McLeod, C. Schwarz, M. Goldflam, M. Liu, J. Kerbusch, R. Nawrodt, S. Ramanathan, D. N. Basov, F. Capasso, C. Ronning, M. A. Kats, *Nano Lett.* **2016**, *16*, 1050.
- [33] G. Dominguez, A. S. McLeod, Z. Gainsforth, P. Kelly, H. A. Bechtel, F. Keilmann, A. Westphal, M. Thiemens, D. N. Basov, *Nat. Commun.* **2014**, *5*, 5445.
- [34] B. K. J. Rosenfeld, in *Climate Change 2013—Physical Science Basis* (Ed: Intergovernmental Panel on Climate Change), Cambridge University Press, Cambridge **1935**, pp. 1–30.
- [35] C. R. Burch, J. P. P. Stock, *J. Sci. Instrum.* **1942**, *19*, 71.
- [36] W. Lang, *ZEISS Inf.* **1968**, *70*, 114.
- [37] M. J. Solomon, M. Kogan, *Encycl. Condens. Matter Phys.* **2005**, *1*, 229.
- [38] E. Wolf, M. Nieto-Vesperinas, *J. Opt. Soc. Am. A* **1985**, *2*, 886.
- [39] B. Knoll, F. Keilmann, *Opt. Commun.* **2000**, *182*, 321.
- [40] M. Dressel, G. Gruener, G. F. Bertsch, *Am. J. Phys.* **2002**, *70*, 1269.
- [41] C. Girard, C. Joachim, S. Gauthier, *Rep. Prog. Phys.* **2000**, *63*, 893.
- [42] C. Girard, A. Dereux, *Rep. Prog. Phys.* **1996**, *59*, 657.
- [43] C. Girard, *Rep. Prog. Phys.* **2005**, *68*, 1883.
- [44] T. G. Rochow, E. G. Rochow, in *An Introd. to Microsc. by Means Light. Electrons, X-Rays, or Ultrasound*, Springer US, Boston, MA **1978**, pp. 273–298.
- [45] G. Binnig, H. Rohrer, C. Gerber, E. Weibel, *Phys. Rev. Lett.* **1982**, *49*, 57.
- [46] D. B. Williams, C. B. Carter, *Transmission Electron Microscopy: A Textbook for Materials Science*, Springer, USA **2009**.
- [47] Z. Fei, G. O. Andreev, W. Bao, L. M. Zhang, A. S. McLeod, C. Wang, M. K. Stewart, Z. Zhao, G. Dominguez, M. Thiemens, M. M. Fogler, M. J. Tauber, A. H. Castro-Neto, C. N. Lau, F. Keilmann, D. N. Basov, *Nano Lett.* **2011**, *11*, 4701.
- [48] J. Crawford, J. Brown, *Libr. Hist.* **2007**, *23*, 267.
- [49] S. Mastel, M. B. Lundeberg, P. Alonso-González, Y. Gao, K. Watanabe, T. Taniguchi, J. Hone, F. H. L. Koppens, A. Y. Nikitin, R. Hillenbrand, *Nano Lett.* **2017**, *17*, 6526.
- [50] P. Ginzburg, D. J. Roth, M. E. Nasir, P. Segovia, A. V. Krasavin, J. Levitt, L. M. Hirvonen, B. Wells, K. Suhling, D. Richards, V. A. Podolskiy, A. V. Zayats, *Light: Sci. Appl.* **2017**, *6*, e16273.
- [51] L. D. Landau, E. M. Lifshitz, L. P. Pitaevskii, *Electrodynamics of Continuous Media*, Elsevier **1984**.
- [52] R. Brown, N. R. Walet, F. Guinea, *Phys. Rev. Lett.* **2018**, *120*, 026802.
- [53] M. B. Lundeberg, Y. Gao, R. Asgari, C. Tan, B. Van Duppen, M. Autore, P. Alonso-González, A. Woessner, K. Watanabe, T. Taniguchi, R. Hillenbrand, J. Hone, M. Polini, F. H. L. Koppens, *Science* **2017**, *357*, 187.
- [54] F. Keilmann, R. Hillenbrand, *Philos. Trans. R. Soc. London. Ser. A* **2004**, *362*, 787.
- [55] S. Patane, P. G. Gucciardi, M. Labardi, M. Allegrini, *Riv. Nuovo Cimento* **2004**, *27*, 1.
- [56] B. T. Rosner, D. W. van der Weide, *Rev. Sci. Instrum.* **2002**, *73*, 2505.
- [57] D. Courjon, C. Bainier, *Rep. Prog. Phys.* **1994**, *57*, 989.
- [58] E. Bründermann, M. Havenith, *Annu. Rep. Prog. Chem., Sect. C: Phys. Chem.* **2008**, *104*, 235.
- [59] A. Centrone, *Annu. Rev. Anal. Chem.* **2015**, *8*, 101.
- [60] W. Adams, M. Sadatgol, D. Ö. Güney, *AIP Adv.* **2016**, *6*, 100701.
- [61] E. Synge, *London, Edinburgh Dublin Philos. Mag. J. Sci.* **1928**, *6*, 356.
- [62] E. H. Synge, *London, Edinburgh Dublin Philos. Mag. J. Sci.* **1932**, *13*, 297.
- [63] J. A. O’Keefe, *J. Opt. Soc. Am.* **1956**, *46*, 359.
- [64] J. Wessel, *J. Opt. Soc. Am. B* **1985**, *2*, 1538.
- [65] K. Karrai, R. D. Grober, *Ultramicroscopy* **1995**, *61*, 197.
- [66] D. W. Pohl, W. Denk, M. Lanz, *Appl. Phys. Lett.* **1984**, *44*, 651.
- [67] U. Dürig, D. W. Pohl, F. Rohner, *J. Appl. Phys.* **1986**, *59*, 3318.
- [68] E. Betzig, A. Lewis, A. Harootunian, M. Isaacson, E. Kratschmer, *Biophys. J.* **1986**, *49*, 269.
- [69] E. Betzig, J. K. Trautman, *Science* **1992**, *257*, 189.
- [70] E. Betzig, A. Harootunian, A. Lewis, M. Isaacson, *Appl. Opt.* **1986**, *25*, 1890.
- [71] E. Ash, G. Nicholls, *Nature* **1972**, *237*, 510.
- [72] A. Lewis, M. Isaacson, A. Harootunian, A. Muray, *Ultramicroscopy* **1984**, *13*, 227.
- [73] E. Betzig, *Rev. Mod. Phys.* **2015**, *87*, 1153.
- [74] B. Hecht, B. Sick, U. P. Wild, V. Deckert, R. Zenobi, O. J. F. Martin, D. W. Pohl, *J. Chem. Phys.* **2000**, *112*, 7761.
- [75] R. Ivanov, S. Marcinkevičius, M. D. Mensi, O. Martinez, L. Y. Kuritzky, D. J. Myers, S. Nakamura, J. S. Speck, *Phys. Rev. Appl.* **2017**, *7*, 064033.
- [76] Y. T. Chen, K. F. Karlsson, J. Birch, P. O. Holtz, *Sci. Rep.* **2016**, *6*, 21482.
- [77] Y. Lee, S. J. Yun, Y. Kim, M. S. Kim, G. H. Han, A. K. Sood, J. Kim, *Nanoscale* **2017**, *9*, 2272.
- [78] Z. Cao, M. Ermes, S. Lehnen, R. Carius, K. Bittkau, *Phys. Chem. Chem. Phys.* **2018**, *20*, 1098.
- [79] Y. Y. H. Lee, S. Park, H. Kim, G. H. Han, Y. Y. H. Lee, J. Kim, *Nanoscale* **2015**, *7*, 11909.
- [80] S. Baral, A. Rafiei Miandashti, H. H. Richardson, *Nanoscale* **2018**, *10*, 941.
- [81] S. Ezugwu, S. Kazemian, D.-Y. W. Choi, G. Fanchini, *Nanoscale* **2017**, *9*, 4097.
- [82] A. C. Jones, M. B. Raschke, *Nano Lett.* **2012**, *12*, 1475.
- [83] S. Ezugwu, H. Ye, G. Fanchini, *Nanoscale* **2015**, *7*, 252.

- [84] D. Denkova, N. Verellen, A. V. Silhanek, V. K. Valev, P. Van Dorpe, V. V. Moshchalkov, *ACS Nano* **2013**, *7*, 3168.
- [85] E. U. Haq, Z. Liu, Y. Zhang, S. A. A. Ahmad, L.-S. Wong, S. P. Armes, J. K. Hobbs, G. J. Leggett, J. Micklefield, C. J. Roberts, J. M. R. Weaver, *Nano Lett.* **2010**, *10*, 4375.
- [86] Y. Nishiyama, H. Okamoto, *J. Phys. Chem. C* **2016**, *120*, 28157.
- [87] H. Mizobata, S. Hasegawa, K. Imura, *J. Phys. Chem. C* **2017**, *121*, 11733.
- [88] Y. Kawakami, A. Kaneta, A. Hashiya, M. Funato, *Phys. Rev. Appl.* **2016**, *6*, 044018.
- [89] J. Nozaki, M. Fukumura, T. Aoki, Y. Maniwa, Y. Yomogida, K. Yanagi, *Sci. Rep.* **2017**, *7*, 46004.
- [90] R.-H. Jiang, C. Chen, D.-Z. Lin, H.-C. Chou, J.-Y. Chu, T.-J. Yen, *Nano Lett.* **2018**, *18*, 881.
- [91] M. Kim, S. Choi, J.-H. Lee, C. Park, T.-H. Chung, J. H. Baek, Y.-H. Cho, *Sci. Rep.* **2017**, *7*, 42221.
- [92] K. Imaeda, S. Hasegawa, K. Imura, *J. Phys. Chem. C* **2018**, *122*, 7399.
- [93] S. Hunsche, M. Koch, I. Brener, M. Nuss, *Opt. Commun.* **1998**, *150*, 22.
- [94] A. Lahrech, R. Bachelot, P. Gleyzes, A. C. Boccarda, *Opt. Lett.* **1996**, *21*, 1315.
- [95] B. Knoll, F. Keilmann, *Nature* **1999**, *399*, 134.
- [96] R. Hillenbrand, T. Taubner, F. Keilmann, *Nature* **2002**, *418*, 159.
- [97] L. Novotny, B. Hecht, *Principles of Nano-Optics*, Cambridge University Press, Cambridge **2006**.
- [98] O. Cathabard, R. Teissier, J. Devenson, J. C. Moreno, A. N. Baranov, *Appl. Phys. Lett.* **2010**, *96*, 141110.
- [99] C. Walther, M. Fischer, G. Scalari, R. Terazzi, N. Hoyler, J. Faist, *Appl. Phys. Lett.* **2007**, *91*, 131122.
- [100] J. M. Atkin, S. Berweger, A. C. Jones, M. B. Raschke, *Adv. Phys.* **2012**, *61*, 745.
- [101] A. C. Jones, S. Berweger, J. Wei, D. Cobden, M. B. Raschke, *Nano Lett.* **2010**, *10*, 1574.
- [102] M. K. Liu, M. Wagner, E. Abreu, S. Kittiwatanakul, A. McLeod, Z. Fei, M. Goldflam, S. Dai, M. M. Fogler, J. Lu, S. A. Wolf, R. D. Averitt, D. N. Basov, *Phys. Rev. Lett.* **2013**, *111*, 096602.
- [103] A. Charnukha, A. Cvitkovic, T. Prokscha, D. Pröpper, N. Ocelic, A. Suter, Z. Salman, E. Morenzoni, J. Deisenhofer, V. Tsurkan, A. Loidl, B. Keimer, A. V. Boris, *Phys. Rev. Lett.* **2012**, *109*, 017003.
- [104] M. Liu, M. Wagner, J. Zhang, A. McLeod, S. Kittiwatanakul, Z. Fei, E. Abreu, M. Goldflam, A. J. Sternbach, S. Dai, K. G. West, J. Lu, S. A. Wolf, R. D. Averitt, D. N. Basov, *Appl. Phys. Lett.* **2014**, *104*, 1.
- [105] M. Liu, A. J. Sternbach, D. N. Basov, *Rep. Prog. Phys.* **2017**, *80*, 014501.
- [106] M. Liu, A. J. Sternbach, M. Wagner, T. V. Slusar, T. Kong, S. L. Bud, S. Kittiwatanakul, M. M. Qazilbash, A. McLeod, Z. Fei, E. Abreu, J. Zhang, M. Goldflam, S. Dai, G. Ni, J. Lu, H. A. Bechtel, M. C. Martin, M. B. Raschke, R. D. Averitt, S. A. Wolf, H. Kim, P. C. Canfield, D. N. Basov, *Phys. Rev. B* **2015**, *91*, 245155.
- [107] X. Lu, O. Khatib, X. Du, J. Duan, W. Wei, X. Liu, H. A. Bechtel, F. D'Apuzzo, M. Yan, A. Buyanin, Q. Fu, J. Chen, M. Salmeron, J. Zeng, M. B. Raschke, P. Jiang, X. Bao, *Adv. Electron. Mater.* **2018**, *4*, 1700377.
- [108] J. Döring, H.-G. von Ribbeck, M. Fehrenbacher, S. C. Kehr, L. M. Eng, *Appl. Phys. Lett.* **2014**, *105*, 053109.
- [109] T. J. Huffman, D. J. Lahneman, S. L. Wang, T. Slusar, B.-J. Kim, H.-T. Kim, M. M. Qazilbash, *Phys. Rev. B* **2018**, *97*, 085146.
- [110] A. J. Frenzel, A. S. McLeod, D. Z.-R. Wang, Y. Liu, W. Lu, G. Ni, A. W. Tsen, Y. Sun, A. N. Pasupathy, D. N. Basov, *Phys. Rev. B* **2018**, *97*, 035111.
- [111] S. N. Gilbert Corder, X. Chen, S. Zhang, F. Hu, J. Zhang, Y. Luan, J. A. Logan, T. Ciavatti, H. A. Bechtel, M. C. Martin, M. Aronson, H. S. Suzuki, S. Kimura, T. Iizuka, Z. Fei, K. Imura, N. K. Sato, T. H. Tao, M. Liu, *Nat. Commun.* **2017**, *8*, 2262.
- [112] S. N. Gilbert Corder, J. Jiang, X. Chen, S. Kittiwatanakul, I.-C. Tung, Y. Zhu, J. Zhang, H. A. Bechtel, M. C. Martin, G. L. Carr, J. Lu, S. A. Wolf, H. Wen, T. H. Tao, M. Liu, *Phys. Rev. B* **2017**, *96*, 161110.
- [113] M. M. Qazilbash, M. Brehm, G. O. Andreev, A. Frenzel, P.-C. Ho, B.-G. Chae, B.-J. Kim, S. J. Yun, H.-T. Kim, A. V. Balatsky, O. G. Shpyrko, M. B. Maple, F. Keilmann, D. N. Basov, *Phys. Rev. B* **2009**, *79*, 075107.
- [114] A. Frenzel, M. M. Qazilbash, M. Brehm, B.-G. Chae, B.-J. Kim, H.-T. Kim, A. V. Balatsky, F. Keilmann, D. N. Basov, *Phys. Rev. B* **2009**, *80*, 115115.
- [115] Q. Jia, J. Grenzer, H. He, W. Anwand, Y. Ji, Y. Yuan, K. Huang, T. You, W. Yu, W. Ren, X. Chen, M. Liu, S. Facsko, X. Wang, X. Ou, *Adv. Mater. Interfaces* **2018**, *5*, 1701268.
- [116] A. Pustogov, A. S. McLeod, Y. Saito, D. N. Basov, M. Dressel, *Sci. Adv.* **2018**, *4*, eaau9123.
- [117] K. W. Post, A. S. McLeod, M. Hepting, M. Bluschke, Y. Wang, G. Cristiani, G. Logvenov, A. Charnukha, G. X. Ni, P. Radhakrishnan, M. Minola, A. Pasupathy, A. V. Boris, E. Benckiser, K. A. Dahmen, E. W. Carlson, B. Keimer, D. N. Basov, *Nat. Phys.* **2018**, *14*, 1056.
- [118] J. Zhang, A. S. McLeod, Q. Han, X. Chen, H. A. Bechtel, Z. Yao, S. N. Gilbert Corder, T. Ciavatti, T. H. Tao, M. Aronson, G. L. Carr, M. C. Martin, C. Sow, S. Yonezawa, F. Nakamura, I. Terasaki, D. N. Basov, A. J. Millis, Y. Maeno, M. Liu, *Phys. Rev. X* **2019**, *9*, 011032.
- [119] K. S. Kim, D. Trajanoski, K. Ho, L. Gilburd, A. Maiti, L. van der Velden, S. De Beer, G. C. Walker, *J. Phys. Chem. Lett.* **2017**, *8*, 2902.
- [120] F. J. Alfaro-Mozaz, P. Alonso-González, S. Vélez, I. Dolado, M. Autore, S. Mastel, F. Casanova, L. E. Hueso, P. Li, A. Y. Nikitin, R. Hillenbrand, *Nat. Commun.* **2017**, *8*, 15624.
- [121] J. Ehlermann, S. Fohrmann, J. Siebels, S. Mendach, *Phys. Rev. B* **2015**, *91*, 235404.
- [122] B. Y. Jiang, G. X. Ni, C. Pan, Z. Fei, B. Cheng, C. N. Lau, M. Bockrath, D. N. Basov, M. M. Fogler, *Phys. Rev. Lett.* **2016**, *117*, 1.
- [123] Z. Fei, E. G. Iwinski, G. X. Ni, L. M. Zhang, W. Bao, A. S. Rodin, Y. Lee, M. Wagner, M. K. Liu, S. Dai, M. D. Goldflam, M. Thiemens, F. Keilmann, C. N. Lau, A. H. Castro-Neto, M. M. Fogler, D. N. Basov, *Nano Lett.* **2015**, *15*, 4973.
- [124] Z. Fei, A. S. Rodin, W. Gannett, S. Dai, W. Regan, M. Wagner, M. K. K. Liu, A. S. S. McLeod, G. Dominguez, M. Thiemens, A. H. H. Castro Neto, F. Keilmann, A. Zettl, R. Hillenbrand, M. M. M. Fogler, D. N. N. Basov, *Nat. Nanotechnol.* **2013**, *8*, 821.
- [125] Z. Fei, M. D. Goldflam, J.-S. Wu, S. Dai, M. Wagner, A. S. McLeod, M. K. Liu, K. W. Post, S. Zhu, G. C. A. M. Janssen, M. M. Fogler, D. N. Basov, *Nano Lett.* **2015**, *15*, 8271.
- [126] S. Dai, Q. Ma, M. K. Liu, T. Andersen, Z. Fei, M. D. Goldflam, M. Wagner, K. Watanabe, T. Taniguchi, M. Thiemens, F. Keilmann, G. C. Janssen, S.-E. Zhu, P. Jarillo-Herrero, M. M. Fogler, D. N. Basov, *Nat. Nanotechnol.* **2015**, *10*, 682.
- [127] Y. Bao, S. Zu, W. Liu, L. Zhou, X. Zhu, Z. Fang, *Phys. Rev. B* **2017**, *95*, 081406.
- [128] J. A. Gerber, S. Berweger, B. T. O'Callahan, M. B. Raschke, *Phys. Rev. Lett.* **2014**, *113*, 055502.
- [129] A. Woessner, M. B. Lundeberg, Y. Gao, A. Principi, P. Alonso-González, M. Carrega, K. Watanabe, T. Taniguchi, G. Vignale, M. Polini, J. Hone, R. Hillenbrand, F. H. L. Koppens, *Nat. Mater.* **2015**, *14*, 421.
- [130] Z. Shi, H. A. Bechtel, S. Berweger, Y. Sun, B. Zeng, C. Jin, H. Chang, M. C. Martin, M. B. Raschke, F. Wang, *ACS Photonics* **2015**, *2*, 790.

- [131] X. G. Xu, J. H. Jiang, L. Gilburd, R. G. Rensing, K. S. Burch, C. Zhi, Y. Bando, D. Golberg, G. C. Walker, *ACS Nano* **2014**, *8*, 11305.
- [132] X. G. Xu, A. E. Tanur, G. C. Walker, *J. Phys. Chem. A* **2013**, *117*, 3348.
- [133] F. Hu, Y. Luan, M. E. Scott, J. Yan, D. G. Mandrus, X. Xu, Z. Fei, *Nat. Photonics* **2017**, *11*, 356.
- [134] D. Hu, X. Yang, C. Li, R. Liu, Z. Yao, H. Hu, S. N. G. Corder, J. Chen, Z. Sun, M. Liu, Q. Dai, *Nat. Commun.* **2017**, *8*, 1471.
- [135] T. Low, A. Chaves, J. D. Caldwell, A. Kumar, N. X. Fang, P. Avouris, T. F. Heinz, F. Guinea, L. Martin-Moreno, F. Koppens, *Nat. Mater.* **2017**, *16*, 182.
- [136] J.-H. Jiang, X. G. Xu, L. Gilburd, G. C. Walker, *Opt. Express* **2017**, *25*, 25059.
- [137] D. N. Basov, M. M. Fogler, F. J. Garcia de Abajo, *Science* **2016**, *354*, aag1992.
- [138] P. Li, I. Dolado, F. J. Alfaro-Mozaz, F. Casanova, L. E. Hueso, S. Liu, J. H. Edgar, A. Y. Nikitin, S. Vélez, R. Hillenbrand, *Science* **2018**, *359*, 892.
- [139] F. J. Bezares, A. De Sanctis, J. R. M. Saavedra, A. Woessner, P. Alonso-González, I. Amenabar, J. Chen, T. H. Bointon, S. Dai, M. M. Fogler, D. N. Basov, R. Hillenbrand, M. F. Craciun, F. J. García de Abajo, S. Russo, F. H. L. Koppens, *Nano Lett.* **2017**, *17*, 5908.
- [140] Z. Shi, X. Hong, H. A. Bechtel, B. Zeng, M. C. Martin, K. Watanabe, T. Taniguchi, Y.-R. Shen, F. Wang, *Nat. Photonics* **2015**, *9*, 515.
- [141] E. Yoxall, M. Schnell, A. Y. Nikitin, O. Txoperena, A. Woessner, M. B. Lundeberg, F. Casanova, L. E. Hueso, F. H. L. Koppens, R. Hillenbrand, *Nat. Photonics* **2015**, *9*, 674.
- [142] J. Duan, R. Chen, Y. Cheng, T. Yang, F. Zhai, Q. Dai, J. Chen, *Adv. Mater.* **2018**, *30*, 1800367.
- [143] A. M. Dubrovkin, B. Qiang, H. N. S. Krishnamoorthy, N. I. Zheludev, Q. J. Wang, *Nat. Commun.* **2018**, *9*, 1762.
- [144] A. Woessner, Y. Gao, I. Torre, M. B. Lundeberg, C. Tan, K. Watanabe, T. Taniguchi, R. Hillenbrand, J. Hone, M. Polini, F. H. L. Koppens, *Nat. Photonics* **2017**, *11*, 421.
- [145] Q. Xu, T. Ma, M. Danesh, B. N. Shivananju, S. Gan, J. Song, C.-W. Qiu, H.-M. Cheng, W. Ren, Q. Bao, *Light: Sci. Appl.* **2017**, *6*, e16204.
- [146] Z. Zheng, J. Chen, Y. Wang, X. Wang, X. Chen, P. Liu, J. Xu, W. Xie, H. Chen, S. Deng, N. Xu, *Adv. Mater.* **2018**, *30*, 1705318.
- [147] S. Dai, M. Tymchenko, Z.-Q. Xu, T. T. Tran, Y. Yang, Q. Ma, K. Watanabe, T. Taniguchi, P. Jarillo-Herrero, I. Aharonovich, D. N. Basov, T. Tao, A. Alu, *Nano Lett.* **2018**, *18*, 5205.
- [148] Z. Fei, J. J. Foley, W. Gannett, M. K. Liu, S. Dai, G. X. Ni, A. Zettl, M. M. Fogler, G. P. Wiederrecht, S. K. Gray, D. N. Basov, *Nano Lett.* **2016**, *16*, 7842.
- [149] M. Tamagnone, A. Ambrosio, K. Chaudhary, L. A. Jauregui, P. Kim, W. L. Wilson, F. Capasso, *Sci. Adv.* **2018**, *4*, eaat7189.
- [150] G. Cheng, D. Wang, S. Dai, X. Fan, F. Wu, X. Li, C. Zeng, *Nanoscale* **2018**, *10*, 16314.
- [151] B.-Y. Jiang, G.-X. Ni, Z. Addison, J. K. Shi, X. Liu, S. Y. F. Zhao, P. Kim, E. J. Mele, D. N. Basov, M. M. Fogler, *Nano Lett.* **2017**, *17*, 7080.
- [152] S. Dai, J. Quan, G. Hu, C. Qiu, T. Tao, X. Li, A. Alu, *Nano Lett.* **2019**, *19*, 1009.
- [153] W. Ma, P. Alonso-González, S. Li, A. Y. Nikitin, J. Yuan, J. Martín-Sánchez, J. Taboada-Gutiérrez, I. Amenabar, P. Li, S. Vélez, C. Tollan, Z. Dai, Y. Zhang, S. Sriram, K. Kalantar-Zadeh, S.-T. Lee, R. Hillenbrand, Q. Bao, *Nature* **2018**, *562*, 557.
- [154] S. S. Sunko, G. X. Ni, B. Y. Jiang, H. Yoo, A. Sternbach, A. S. McLeod, T. Stauber, L. Xiong, T. Taniguchi, K. Watanabe, P. Kim, M. M. Fogler, D. N. Basov, *Science* **2018**, *362*, 1153.
- [155] Y. Zhou, R. Chen, J. Wang, Y. Huang, M. Li, Y. Xing, J. Duan, J. Chen, J. D. Farrell, H. Q. Xu, J. Chen, *Adv. Mater.* **2018**, *30*, 1802551.
- [156] P. Li, X. Yang, T. W. W. Maß, J. Hanss, M. Lewin, A.-K. U. Michel, M. Wuttig, T. Taubner, *Nat. Mater.* **2016**, *15*, 870.
- [157] R. Hillenbrand, F. Keilmann, *Appl. Phys. Lett.* **2002**, *80*, 25.
- [158] J. M. Stiegler, Y. Abate, A. Cvitkovic, Y. E. Romanyuk, A. J. Huber, S. R. Leone, R. Hillenbrand, *ACS Nano* **2011**, *5*, 6494.
- [159] J. Chen, P. Albella, Z. Pirzadeh, P. Alonso-González, F. Huth, S. Bonetti, V. Bonanni, J. Åkerman, J. Nogués, P. Vavassori, A. Dmitriev, J. Aizpurua, R. Hillenbrand, *Small* **2011**, *7*, 2341.
- [160] Z. Nuño, B. Hessler, B. Heiberg, R. Damato, T. Dunlap, Y.-S. Shon, Y. Abate, *J. Nanopart. Res.* **2012**, *14*, 776.
- [161] A. García-Etxarri, I. Romero, F. J. García de Abajo, R. Hillenbrand, J. Aizpurua, *Phys. Rev. B* **2009**, *79*, 125439.
- [162] D.-S. Kim, Z. H. Kim, *Opt. Express* **2012**, *20*, 8689.
- [163] P. Alonso-González, P. Albella, F. Neubrech, C. Huck, J. Chen, F. Golmar, F. Casanova, L. E. Hueso, A. Pucci, J. Aizpurua, R. Hillenbrand, *Phys. Rev. Lett.* **2013**, *110*, 1.
- [164] J. A. Schuller, E. S. Barnard, W. Cai, Y. C. Jun, J. S. White, M. L. Brongersma, *Nat. Mater.* **2010**, *9*, 193.
- [165] R. Hillenbrand, F. Keilmann, *Appl. Phys. B* **2001**, *73*, 239.
- [166] P. Alonso-Gonzalez, M. Schnell, P. Sarriugarte, H. Sobhani, C. Wu, N. Arju, A. Khanikaev, F. Golmar, P. Albella, L. Arzubiaga, F. Casanova, L. E. Hueso, P. Nordlander, G. Shvets, R. Hillenbrand, *Nano Lett.* **2011**, *11*, 3922.
- [167] M. Rahmani, E. Yoxall, B. Hopkins, Y. Sonnefraud, Y. Kivshar, M. Hong, C. Phillips, S. A. Maier, A. E. Miroshnichenko, *ACS Nano* **2013**, *7*, 11138.
- [168] W. Chen, A. Kimel, A. Kirilyuk, T. Rasing, *Phys. Status Solidi B* **2010**, *247*, 2047.
- [169] Y. Xu, E. Tucker, G. Boreman, M. B. Raschke, B. A. Lail, *ACS Photonics* **2016**, *3*, 881.
- [170] J. Dorfmüller, D. Dregely, M. Esslinger, W. Khunsin, R. Vogelgesang, K. Kern, H. Giessen, *Nano Lett.* **2011**, *11*, 2819.
- [171] T. G. Habteyes, *J. Phys. Chem. C* **2014**, *118*, 9119.
- [172] S. E. Grefe, D. Leiva, S. Mastel, S. D. Dhuey, S. Cabrini, P. J. Schuck, Y. Abate, *Phys. Chem. Chem. Phys.* **2013**, *15*, 18944.
- [173] H. T. Stinson, J. S. Wu, B. Y. Jiang, Z. Fei, A. S. Rodin, B. C. Chapler, A. S. McLeod, A. Castro Neto, Y. S. Lee, M. M. Fogler, D. N. Basov, *Phys. Rev. B* **2014**, *90*, 014502.
- [174] A. Arcangeli, F. Rossella, A. Tomadin, J. Xu, D. Ercolani, L. Sorba, F. Beltram, A. Tredicucci, M. Polini, S. Rodaro, *Nano Lett.* **2016**, *16*, 5688.
- [175] V. Suresh, L. Ding, A. B. Chew, F. L. Yap, *ACS Appl. Nano Mater.* **2018**, *1*, 886.
- [176] E. Ostrovsky, K. Cohen, S. Tsesses, B. Gjonaj, G. Bartal, *Optica* **2018**, *5*, 283.
- [177] Y. Sang, X. Wu, S. S. Raja, C.-Y. Wang, H. Li, Y. Ding, D. Liu, J. Zhou, H. Ahn, S. Gwo, J. Shi, *Adv. Opt. Mater.* **2018**, *6*, 1701368.
- [178] N. F. Mott, *Rev. Mod. Phys.* **1968**, *40*, 677.
- [179] E. Dagotto, *Science* **2005**, *309*, 257.
- [180] B. T. O'Callahan, M. B. Raschke, *APL Photonics* **2017**, *2*, 021301.
- [181] A. A. Govyadinov, S. Mastel, F. Golmar, A. Chuvilin, P. S. Carney, R. Hillenbrand, *ACS Nano* **2014**, *8*, 6911.
- [182] A. A. Govyadinov, I. Amenabar, F. Huth, P. S. Carney, R. Hillenbrand, *J. Phys. Chem. Lett.* **2013**, *4*, 1526.
- [183] D. E. Tranca, S. G. Stanciu, R. Hristu, C. Stoichita, S. A. M. Tofail, G. A. Stanciu, *Sci. Rep.* **2015**, *5*, 11876.
- [184] C. Liao, Y. Lo, *J. Opt. Soc. Am. B* **2013**, *30*, 2819.
- [185] D. E. Tranca, S. G. Stanciu, R. Hristu, B. M. Witgen, G. A. Stanciu, *Nanomedicine* **2018**, *14*, 47.
- [186] J. Aizpurua, T. Taubner, F. J. Garcia de Abajo, M. Brehm, R. Hillenbrand, *Opt. Express* **2008**, *16*, 1529.
- [187] P. Li, T. Wang, H. Böckmann, T. Taubner, *Nano Lett.* **2014**, *14*, 4400.

- [188] L. Wang, X. G. Xu, *Nat. Commun.* **2015**, *6*, 8973.
- [189] H. Wang, L. Wang, D. S. Jakob, X. G. Xu, *AIP Adv.* **2017**, *7*, 055118.
- [190] P. Schmidt, F. Vialla, S. Latini, M. Massicotte, K.-J. Tielrooij, S. Mastel, G. Navickaite, M. Danovich, D. A. Ruiz-Tijerina, C. Yelgel, V. Fal'ko, K. S. Thygesen, R. Hillenbrand, F. H. L. Koppens, *Nat. Nanotechnol.* **2018**, *13*, 1035.
- [191] F. Mooshammer, F. Sandner, M. A. Huber, M. Zizlsperger, M. Plankl, C. Weyrich, M. Lanius, J. Kampmeier, D. Grützmacher, J. L. Boland, T. L. Cocker, R. Huber, H. Weigand, M. Plankl, C. Weyrich, M. Lanius, J. Kampmeier, G. Mussler, D. Grützmacher, J. L. Boland, T. L. Cocker, R. Huber, *Nano Lett.* **2018**, *18*, 7515.
- [192] J. Orenstein, *Phys. Today* **2012**, *65*, 44.
- [193] R. Ulbricht, E. Hendry, J. Shan, T. F. Heinz, M. Bonn, *Rev. Mod. Phys.* **2011**, *83*, 543.
- [194] A. J. Sternbach, J. Hinton, T. Slusar, A. S. McLeod, M. K. Liu, A. Frenzel, M. Wagner, R. Iraheta, F. Keilmann, A. Leitenstorfer, M. Fogler, H.-T. Kim, R. D. Averitt, D. N. Basov, *Opt. Express* **2017**, *25*, 28589.
- [195] M. Wagner, Z. Fei, A. S. McLeod, A. S. Rodin, W. Bao, E. G. Iwinski, Z. Zhao, M. Goldflam, M. Liu, G. Dominguez, M. Thiemens, M. N. Fogler, A. H. Castro Neto, C. N. Lau, S. Amarie, F. Keilmann, D. N. Basov, *Nano Lett.* **2014**, *14*, 894.
- [196] M. Wagner, A. S. McLeod, S. J. Maddox, Z. Fei, M. Liu, R. D. Averitt, M. M. Fogler, S. R. Bank, F. Keilmann, D. N. Basov, *Nano Lett.* **2014**, *14*, 4529.
- [197] B. T. O'Callahan, A. C. Jones, J. Hyung Park, D. H. Cobden, J. M. Atkin, M. B. Raschke, *Nat. Commun.* **2015**, *6*, 6849.
- [198] S. A. Dönges, O. Khatib, B. T. O'Callahan, J. M. Atkin, J. H. Park, D. Cobden, M. B. Raschke, *Nano Lett.* **2016**, *16*, 3029.
- [199] M. Eisele, T. L. Cocker, M. A. Huber, M. Plankl, L. Viti, D. Ercolani, L. Sorba, M. S. Vitiello, R. Huber, *Nat. Photonics* **2014**, *8*, 841.
- [200] G. X. Ni, L. Wang, M. D. Goldflam, M. Wagner, Z. Fei, A. S. McLeod, M. K. Liu, F. Keilmann, B. Özyilmaz, A. H. Castro Neto, J. Hone, M. M. Fogler, D. N. Basov, *Nat. Photonics* **2016**, *10*, 244.
- [201] H. Wang, L. Wang, X. G. Xu, *Nat. Commun.* **2016**, *7*, 13212.
- [202] R. Jacob, S. Winnerl, H. Schneider, M. Helm, M. T. Wenzel, H.-G. von Ribbeck, L. M. Eng, S. C. Kehr, *Opt. Express* **2010**, *18*, 26206.
- [203] J. Mattis Hoffmann, B. Hauer, T. Taubner, *Appl. Phys. Lett.* **2012**, *101*, 193105.
- [204] P. Hermann, A. Hoehl, P. Patoka, F. Huth, E. Rühl, G. Ulm, *Opt. Express* **2013**, *21*, 2913.
- [205] C. M. Johnson, M. Böhmeler, *Corros. Sci.* **2016**, *108*, 60.
- [206] P. Hermann, B. Kästner, A. Hoehl, V. Kashcheyevs, P. Patoka, G. Ulrich, J. Feikes, M. Ries, T. Tydecks, B. Beckhoff, E. Rühl, G. Ulm, *Opt. Express* **2017**, *25*, 16574.
- [207] B. Pollard, F. C. B. Maia, M. B. Raschke, R. O. Freitas, *Nano Lett.* **2016**, *16*, 55.
- [208] I. Amenabar, S. Poly, M. Goikoetxea, W. Nuansing, P. Lasch, R. Hillenbrand, *Nat. Commun.* **2017**, *8*, 14402.
- [209] P. Patoka, G. Ulrich, A. E. Nguyen, L. Bartels, P. A. Dowben, V. Turkowski, T. S. Rahman, P. Hermann, B. Kästner, A. Hoehl, G. Ulm, E. Rühl, *Opt. Express* **2016**, *24*, 1154.
- [210] T. Steinle, F. Mörz, A. Steinmann, H. Giessen, *Opt. Lett.* **2016**, *41*, 4863.
- [211] F. Mörz, R. Semenyshyn, T. Steinle, F. Neubrech, U. Zschieschang, H. Klauk, A. Steinmann, H. Giessen, *Opt. Express* **2017**, *25*, 32355.
- [212] T. Steinle, F. Neubrech, A. Steinmann, X. Yin, H. Giessen, **2013**, *157403*, 9005.
- [213] L. M. Zhang, G. O. Andreev, Z. Fei, A. S. McLeod, G. Dominguez, M. Thiemens, A. H. Castro-Neto, D. N. Basov, M. M. Fogler, *Phys. Rev. B* **2012**, *85*, 075419.
- [214] P. Hermann, A. Hoehl, G. Ulrich, C. Fleischmann, A. Hermelink, B. Kästner, P. Patoka, A. Hornemann, B. Beckhoff, E. Rühl, G. Ulm, *Opt. Express* **2014**, *22*, 17948.
- [215] S. Kimura, H. Okamura, *J. Phys. Soc. Jpn.* **2012**, *82*, 1.
- [216] J. Feikes, M. Von Hartrott, M. Ries, P. Schmid, G. Wüstefeld, A. Hoehl, R. Klein, R. Müller, G. Ulm, *Phys. Rev. Spec. Top. – Accel. Beams* **2011**, *14*, 1.
- [217] R. O. Freitas, F. C. B. Maia, C. Deneke, T. Moreno, P. Dumas, H. Westfahl, Y. Petroff, *Synchrotron Radiat. News* **2017**, *30*, 24.
- [218] G. Kamel, S. Lefrançois, M. Al-Najdawi, T. Abu-Hanieh, I. Saleh, Y. Momani, P. Dumas, *Synchrotron Radiat. News* **2017**, *30*, 8.
- [219] R. O. Freitas, C. Deneke, F. C. B. Maia, H. G. Medeiros, T. Moreno, P. Dumas, Y. Petroff, H. Westfahl, *Opt. Express* **2018**, *26*, 11238.
- [220] O. Khatib, H. A. Bechtel, M. C. Martin, M. B. Raschke, G. L. Carr, *ACS Photonics* **2018**, *5*, 2773.
- [221] D. J. Lahneman, T. J. Huffman, P. Xu, S. L. Wang, T. Grogan, M. M. Qazilbash, *Opt. Express* **2017**, *25*, 20421.
- [222] F. Huth, M. Schnell, J. Wittborn, N. Ocelic, R. Hillenbrand, *Nat. Mater.* **2011**, *10*, 352.
- [223] M. Wagner, D. S. Jakob, S. Horne, H. Mittel, S. Osechinskiy, C. Phillips, G. C. Walker, C. Su, X. G. Xu, *ACS Photonics* **2018**, *5*, 1467.
- [224] P. H. Siegel, *IEEE Trans. Microwave Theory Tech.* **2004**, *52*, 2438.
- [225] A. J. Fitzgerald, V. P. Wallace, M. Jimenez-Linan, L. Bobrow, R. J. Pye, A. D. Purushotham, D. D. Arnone, *Radiology* **2006**, *239*, 533.
- [226] C. Jansen, S. Wietzke, O. Peters, M. Scheller, N. Vieweg, M. Salhi, N. Krumbholz, C. Jördens, T. Hochrein, M. Koch, *Appl. Opt.* **2010**, *49*, E48.
- [227] Z. Zhou, T. Zhou, S. Zhang, Z. Shi, Y. Chen, W. Wan, X. Li, X. Chen, S. N. Gilbert Corder, Z. Fu, L. Chen, Y. Mao, J. Cao, F. G. Omenetto, M. Liu, H. Li, T. H. Tao, *Adv. Sci.* **2018**, *5*, 1700982.
- [228] R. A. Lewis, *Proc. IEEE* **2007**, *95*, 1641.
- [229] D. W. Faries, P. L. Richards, Y. R. Shen, K. H. Yang, *Phys. Rev. A* **1971**, *3*, 2148.
- [230] Q. Y. Lu, N. Bandyopadhyay, S. Slivken, Y. Bai, M. Razeghi, *Appl. Phys. Lett.* **2013**, *103*, 231110.
- [231] B. S. Williams, S. Kumar, H. Callebaut, J. L. Reno, *16th Annu. Meet. IEEE Lasers Electro-Opt. Soc.* **2003**, *1*, 342.
- [232] S. Kumar, B. S. Williams, S. Kohen, Q. Hu, J. L. Reno, *Appl. Phys. Lett.* **2004**, *84*, 2494.
- [233] K. Wang, D. M. Mittleman, N. C. J. van der Valk, P. C. M. Planken, *Appl. Phys. Lett.* **2004**, *85*, 2715.
- [234] H. Zhan, V. Astley, M. Hvasta, J. A. Deibel, D. M. Mittleman, Y. S. Lim, *Appl. Phys. Lett.* **2007**, *91*, 2.
- [235] K. Wang, A. Barkan, D. M. Mittleman, *Appl. Phys. Lett.* **2004**, *84*, 305.
- [236] V. Astley, H. Zhan, R. Mendis, D. M. Mittleman, *J. Appl. Phys.* **2009**, *105*, 113117.
- [237] H. Zhan, R. Mendis, D. M. Mittleman, *J. Opt. Soc. Am. B* **2011**, *28*, 558.
- [238] J. Liu, R. Mendis, D. M. Mittleman, N. Sakoda, *Appl. Phys. Lett.* **2012**, *100*, 031101.
- [239] H.-G. von Ribbeck, M. Brehm, D. W. van der Weide, S. Winnerl, O. Drachenko, M. Helm, F. Keilmann, *Opt. Express* **2008**, *16*, 3430.
- [240] R. Jacob, S. Winnerl, M. Fehrenbacher, J. Bhattacharyya, H. Schneider, M. T. Wenzel, H.-G. von Ribbeck, L. M. Eng, P. Atkinson, O. G. Schmidt, M. Helm, *Nano Lett.* **2012**, *12*, 4336.
- [241] Q. Chen, Z. Jiang, G. X. Xu, X. C. Zhang, *Opt. Lett.* **2000**, *25*, 1122.
- [242] H.-T. Chen, R. Kersting, G. C. Cho, *Appl. Phys. Lett.* **2003**, *83*, 3009.
- [243] P. R. Smith, D. H. Auston, M. C. Nuss, *IEEE J. Quantum Electron.* **1988**, *24*, 255.
- [244] N. Katzenellenbogen, D. Grischkowsky, *Appl. Phys. Lett.* **1991**, *58*, 222.

- [245] Y. C. Shen, P. C. Upadhyaya, H. E. Beere, E. H. Linfield, A. G. Davies, I. S. Gregory, C. Baker, W. R. Tribe, M. J. Evans, *Appl. Phys. Lett.* **2004**, *85*, 164.
- [246] T. Kurihara, K. Yamaguchi, H. Watanabe, M. Nakajima, T. Suemoto, *Appl. Phys. Lett.* **2013**, *103*, 151105.
- [247] J. Zhang, X. Chen, S. Mills, T. Ciavatti, Z. Yao, R. Mescall, H. Hu, V. Semenenko, Z. Fei, H. Li, V. Perebeinos, H. Tao, Q. Dai, X. Du, M. Liu, *ACS Photonics* **2018**, *5*, 2645.
- [248] K. Moon, H. Park, J. Kim, Y. Do, S. Lee, G. Lee, H. Kang, H. Han, *Nano Lett.* **2015**, *15*, 549.
- [249] H. T. Stinson, A. Sternbach, O. Najera, R. Jing, A. S. McLeod, T. V. Slusar, A. Mueller, L. Anderegg, H. T. Kim, M. Rozenberg, D. N. Basov, *Nat. Commun.* **2018**, *9*, 3604.
- [250] C. Liewald, S. Mastel, J. Hesler, A. J. Huber, R. Hillenbrand, F. Keilmann, *Optica* **2018**, *5*, 159.
- [251] M. C. Giordano, S. Mastel, C. Liewald, L. L. Columbo, M. Brambilla, L. Viti, A. Politano, K. Zhang, L. Li, A. G. Davies, E. H. Linfield, R. Hillenbrand, F. Keilmann, G. Scamarcio, M. S. Vitiello, *Opt. Express* **2018**, *26*, 18423.
- [252] R. Degl'Innocenti, R. Wallis, B. Wei, L. Xiao, S. J. Kindness, O. Mitrofanov, P. Braeuninger-Weimer, S. Hofmann, H. E. Beere, D. A. Ritchie, *ACS Photonics* **2017**, *4*, 2150.
- [253] P. Alonso-González, A. Y. Nikitin, Y. Gao, A. Woessner, M. B. Lundberg, A. Principi, N. Forcellini, W. Yan, S. Vélez, A. J. Huber, K. Watanabe, T. Taniguchi, F. Casanova, L. E. Hueso, M. Polini, J. Hone, F. H. L. Koppens, R. Hillenbrand, *Nat. Nanotechnol.* **2016**, *12*, 31.
- [254] P. Klarskov, H. Kim, V. L. Colvin, D. M. Mittleman, *ACS Photonics* **2017**, *4*, 2676.
- [255] H. U. Yang, E. Hebestreit, E. E. Josberger, M. B. Raschke, *Rev. Sci. Instrum.* **2013**, *84*, 023701.
- [256] J. Döring, D. Lang, L. Wehmeier, F. Kuschewski, T. Nörenberg, S. C. Kehr, L. M. Eng, *Nanoscale* **2018**, *10*, 18074.
- [257] G. X. Ni, A. S. McLeod, Z. Sun, L. Wang, L. Xiong, K. W. Post, S. S. Sunku, B.-Y. Jiang, J. Hone, C. R. Dean, M. M. Fogler, D. N. Basov, *Nature* **2018**, *557*, 530.
- [258] K. Lai, M. Nakamura, W. Kundhikanjana, M. Kawasaki, Y. Tokura, M. A. Kelly, Z.-X. Shen, *Science* **2010**, *329*, 190.
- [259] K. Lai, W. Kundhikanjana, M. Kelly, Z. X. Shen, *Rev. Sci. Instrum.* **2008**, *79*, 063703.
- [260] G. Gramse, M. Kasper, L. Fumagalli, G. Gomila, P. Hinterdorfer, F. Kienberger, *Nanotechnology* **2014**, *25*, 145703.
- [261] K. Lai, W. Kundhikanjana, H. Peng, Y. Cui, M. A. Kelly, Z. X. Shen, *Rev. Sci. Instrum.* **2009**, *80*, 043707.
- [262] W. Dickson, S. Takahashi, R. Pollard, R. Atkinson, A. V. Zayats, *J. Microsc.* **2003**, *209*, 194.
- [263] J. N. Walford, J.-A. Porto, R. Carminati, J.-J. Greffet, *J. Opt. Soc. Am. A* **2002**, *19*, 572.
- [264] W. Dickson, A. Stashkevitch, J. Ben Youssef, S. Takahashi, A. V. Zayats, *Opt. Commun.* **2005**, *250*, 126.
- [265] P. L. Stiles, J. A. Dieringer, N. C. Shah, R. P. Van Duyne, *Annu. Rev. Anal. Chem.* **2008**, *1*, 601.
- [266] X. Shi, N. Coca-López, J. Janik, A. Hartschuh, *Chem. Rev.* **2017**, *117*, 4945.
- [267] W. Zhang, Z. Fang, X. Zhu, *Chem. Rev.* **2017**, *117*, 5095.
- [268] F. Pfeiffer, C. David, J. F. van der Veen, C. Bergemann, *Phys. Rev. B* **2006**, *73*, 245331.
- [269] J. Park, Q. Zhang, P. Chen, M. P. Cosgriff, J. A. Tilka, C. Adamo, D. G. Schlom, H. Wen, Y. Zhu, P. G. Evans, *Rev. Sci. Instrum.* **2015**, *86*, 0.
- [270] G. Dai, Z. Yang, G. Geng, M. Li, T. Chang, D. Wei, C. Du, H.-L. Cui, H. Wang, *Appl. Spectrosc. Rev.* **2018**, *4928*, 1.
- [271] B. Deutsch, R. Hillenbrand, L. Novotny, *Opt. Express* **2008**, *16*, 494.
- [272] M. Schnell, P. S. Carney, R. Hillenbrand, *Nat. Commun.* **2014**, *5*, 1.
- [273] B. Deutsch, M. Schnell, R. Hillenbrand, P. S. Carney, *Opt. Express* **2014**, *22*, 26621.
- [274] X. G. Xu, L. Gilburd, G. C. Walker, *Appl. Phys. Lett.* **2014**, *105*, 263104.
- [275] I. Stefanon, S. Blaize, A. Bruyant, S. Aubert, G. Lerondel, R. Bachelot, P. Royer, *Opt. Express* **2005**, *13*, 5553.
- [276] L. Gomez, R. Bachelot, A. Bouhelier, G. P. Wiederrecht, S. Chang, S. K. Gray, F. Hua, S. Jeon, J. A. Rogers, M. E. Castro, S. Blaize, I. Stefanon, G. Lerondel, P. Royer, *J. Opt. Soc. Am. B* **2006**, *23*, 823.
- [277] J. E. Hall, G. P. Wiederrecht, S. K. Gray, S.-H. Chang, S. Jeon, J. A. Rogers, R. Bachelot, P. Royer, *Opt. Express* **2007**, *15*, 4098.
- [278] N. Ocelic, A. Huber, R. Hillenbrand, *Appl. Phys. Lett.* **2006**, *89*, 101124.
- [279] D. E. Tranca, C. Stoichita, R. Hristu, S. G. Stanciu, G. A. Stanciu, *Opt. Express* **2014**, *22*, 1687.
- [280] C. Moreno, J. Alda, E. Kinzel, G. Boreman, *Appl. Opt.* **2017**, *56*, 1037.
- [281] G. W. Ford, W. H. Weber, *Phys. Rep.* **1984**, *113*, 195.
- [282] Z. Fei, Ph.D dissertation, University of California **2015**.
- [283] R. K. Moore, W. E. Blair, *J. Res. Natl. Bur. Stand. Sect. D* **1961**, *65D*, 547.
- [284] P. R. Antoniewicz, *J. Chem. Phys.* **1972**, *56*, 1711.
- [285] P. A. Bobbert, J. Vlieger, *Phys. A* **1986**, *137*, 209.
- [286] B. R. Johnson, *J. Opt. Soc. Am. A* **1992**, *9*, 1341.
- [287] R. Schmehl, B. M. Nebeker, E. D. Hirleman, *J. Opt. Soc. Am. A* **1997**, *14*, 3026.
- [288] P. C. Chaumet, M. Nieto-Vesperinas, *Phys. Rev. B* **2000**, *61*, 14119.
- [289] F. Zenhausern, Y. Martin, H. K. Wickramasinghe, *Science* **1995**, *269*, 1083.
- [290] R. Hillenbrand, F. Keilmann, *Phys. Rev. Lett.* **2000**, *85*, 3029.
- [291] R. Hillenbrand, B. Knoll, F. Keilmann, *J. Microsc.* **2001**, *202*, 77.
- [292] J. Renger, S. Grafström, L. M. Eng, R. Hillenbrand, *Phys. Rev. B* **2005**, *71*, 075410.
- [293] K. Moon, E. Jung, M. Lim, Y. Do, H. Han, *Opt. Express* **2011**, *19*, 11539.
- [294] E. Yoxall, M. Navarro-Cía, M. Rahmani, S. A. Maier, C. C. Phillips, *Appl. Phys. Lett.* **2013**, *103*, 213110.
- [295] C. Bohren, D. Huffman, *Absorption and Scattering of Light by Small Particles*, Wiley-VCH Verlag GmbH, Weinheim, Germany **1998**.
- [296] I. S. Averbukh, B. M. Chernobrod, O. A. Sedletsky, Y. Prior, *Opt. Commun.* **2000**, *174*, 33.
- [297] S. C. Schneider, S. Grafström, L. M. Eng, *Phys. Rev. B* **2005**, *71*, 115418.
- [298] J. A. Porto, P. Johansson, S. P. Apell, T. López-Ríos, *Phys. Rev. B* **2003**, *67*, 085409.
- [299] S. V. Sukhov, *Ultramicroscopy* **2004**, *101*, 111.
- [300] B.-Y. Jiang, N. Ocelic, R. Hillenbrand, *Opt. Express* **2007**, *15*, 8550.
- [301] I. V. Lindell, K. I. Nikoskinen, *J. Electromagn. Waves Appl.* **2001**, *15*, 1075.
- [302] S. Amarie, F. Keilmann, *Phys. Rev. B* **2011**, *83*, 045404.
- [303] A. S. McLeod, P. Kelly, M. D. Goldflam, Z. Gainsforth, A. J. Westphal, G. Dominguez, M. H. Thiemens, M. M. Fogler, D. N. Basov, *Phys. Rev. B* **2014**, *90*, 085136.
- [304] B.-Y. Jiang, L. M. Zhang, A. H. Castro Neto, D. N. Basov, M. M. Fogler, *J. Appl. Phys.* **2016**, *119*, 054305.
- [305] S. T. Chui, X. Chen, M. Liu, Z. Lin, J. Zi, *Phys. Rev. B* **2018**, *97*, 081406.
- [306] X. Chen, C. F. B. Lo, W. Zheng, H. Hu, Q. Dai, M. Liu, *Appl. Phys. Lett.* **2017**, *111*, 223110.
- [307] V. E. Babicheva, S. Gamage, M. I. Stockman, Y. Abate, *Opt. Express* **2017**, *25*, 23935.
- [308] R. Esteban, R. Vogelgesang, K. Kern, *Opt. Express* **2009**, *17*, 2518.
- [309] J. Robertson, *Eur. Phys. J. Appl. Phys.* **2004**, *28*, 265.

- [310] M. Skacel, F. Pagliano, T. Hoang, L. Midolo, S. Fattahpoor, L. Li, E. H. Linfield, A. Fiore, *Phys. Rev. B* **2013**, *88*, 035416.
- [311] A. J. Huber, N. Ocelic, R. Hillenbrand, *J. Microsc.* **2008**, *229*, 389.
- [312] A. Dazzi, C. B. Prater, *Chem. Rev.* **2017**, *117*, 5146.
- [313] M. Pilling, P. Gardner, *Chem. Soc. Rev.* **2016**, *45*, 1935.
- [314] F. S. Ruggeri, G. Longo, S. Faggiano, E. Lipiec, A. Pastore, G. Dietler, *Nat. Commun.* **2015**, *6*, 1.
- [315] J. Chae, Q. Dong, J. Huang, A. Centrone, *Nano Lett.* **2015**, *15*, 8114.
- [316] F. Lu, M. Jin, M. A. Belkin, *Nat. Photonics* **2014**, *8*, 307.
- [317] S. Ghosh, N. A. Kouamé, L. Ramos, S. Remita, A. Dazzi, A. Deniset-Besseau, P. Beaunier, F. Goubard, P. H. Aubert, H. Remita, *Nat. Mater.* **2015**, *14*, 505.
- [318] A. B. Khanikaev, N. Arju, Z. Fan, D. Purtseladze, F. Lu, J. Lee, P. Sarriugarte, M. Schnell, R. Hillenbrand, M. A. Belkin, G. Shvets, *Nat. Commun.* **2016**, *7*, 1.
- [319] R. Dong, Y. Fang, J. Chae, J. Dai, Z. Xiao, Q. Dong, Y. Yuan, A. Centrone, X. C. Zeng, J. Huang, *Adv. Mater.* **2015**, *27*, 1912.
- [320] B. Lahiri, G. Holland, V. Aksyuk, A. Centrone, *Nano Lett.* **2013**, *13*, 3218.
- [321] J. Yang, J. Hatcherian, P. C. Hackley, A. E. Pomerantz, *Nat. Commun.* **2017**, *8*, 2179.
- [322] S. Morsch, P. D. Bastidas, S. M. Rowland, *J. Mater. Chem. A* **2017**, *5*, 24508.
- [323] Z. Liu, K. Nørgaard, M. H. Overgaard, M. Ceccato, D. M. A. Mackenzie, N. Stenger, S. L. S. Stipp, T. Hassenkam, *Carbon* **2018**, *127*, 141.
- [324] A. L. Bondy, R. M. Kirpes, R. L. Merzel, K. A. Pratt, M. M. Banaszak Holl, A. P. Ault, *Anal. Chem.* **2017**, *89*, 8594.
- [325] L. V. Brown, M. Davanco, Z. Sun, A. Kretinin, Y. Chen, J. R. Matson, I. Vurgaftman, N. Sharac, A. J. Giles, M. M. Fogler, T. Taniguchi, K. Watanabe, K. S. Novoselov, S. A. Maier, A. Centrone, J. D. Caldwell, *Nano Lett.* **2018**, *18*, 1628.
- [326] L. Wang, H. Wang, M. Wagner, Y. Yan, D. S. Jakob, X. G. Xu, *Sci. Adv.* **2017**, *3*, e1700255.
- [327] L. Wang, D. Huang, C. K. Chan, Y. J. Li, X. G. Xu, *Chem. Commun.* **2017**, *53*, 7397.
- [328] H. Wang, L. Wang, D. S. Jakob, X. G. Xu, *Nat. Commun.* **2018**, *9*, 2005.
- [329] S. Komiyama, Y. Kajihara, K. Kosaka, T. Ueda, Z. An, *Near-field Nanoscopy of Thermal Evanescent Waves on Metals*, **2016**, Arxiv ID: 1601.00368.
- [330] Q. Weng, S. Komiyama, L. Yang, Z. An, P. Chen, S.-A. Biehs, Y. Kajihara, W. Lu, *Science* **2018**, *360*, 775.
- [331] H. Greener, M. Mrejen, U. Arieli, H. Suchowski, *Opt. Lett.* **2017**, *42*, 3157.
- [332] F. Bilotti, S. Tricarico, F. Pierini, L. Vegni, *Opt. Lett.* **2011**, *36*, 211.
- [333] C. C. Neacsu, S. Berweger, R. L. Olmon, L. V. Saraf, C. Ropers, M. B. Raschke, *Nano Lett.* **2010**, *10*, 592.
- [334] T. Umakoshi, Y. Saito, P. Verma, *Nanoscale* **2016**, *8*, 5634.
- [335] H. T. Chorsi, J. X. J. Zhang, *IEEE Photonics J.* **2017**, *9*, 1.
- [336] T. Tachizaki, T. Nakata, K. Zhang, I. Yamakawa, S. Taniguchi, *Ultra-microscopy* **2018**, *186*, 18.
- [337] E. A. Power, T. Thirunamachandran, *Phys. Rev. A* **1997**, *56*, 3395.
- [338] O. Keller, *Quantum Theory of Near-Field Electrodynamics*, Springer, Berlin, Heidelberg **2011**.